Scattering from a classically chaotic repellor

Pierre Gaspard and Stuart A. Rice

Citation: J. Chem. Phys. **90**, 2225 (1989); doi: 10.1063/1.456017
View online: http://dx.doi.org/10.1063/1.456017
View Table of Contents: http://jcp.aip.org/resource/1/JCPSA6/v90/i4
Published by the American Institute of Physics.

Scattering from a classically chaotic repellor

Pierre Gaspard and Stuart A. Rice
Department of Chemistry and The James Franck Institute, The University of Chicago, Chicago, Illinois 60637

(Received 9 September 1988; accepted 11 November 1988)

We report a study of the classical scattering of a point particle from three hard circular discs in a plane, which we propose as a model of an idealized unimolecular fragmentation. The system possesses a fractal and chaotic metastable classical state. On the basis of a coding of the system dynamics, we develop a method to construct the invariant probability measure and to calculate the particle escape rate, the Hausdorff dimension, the Kolmogorov–Sinai entropy per unit time and the mean largest Lyapunov exponent of the repellor. The relations between these characteristics of the system dynamics are discussed. In particular, we show that, in general, chaos inhibits escaping from the metastable state. The theory is compared with numerical simulations. We also introduce the classical tools necessary for the semiclassical quantization of the dynamics; the latter is discussed in the following paper.

I. INTRODUCTION

Despite the wording of the title, this paper and the following two are concerned with some of the relationships between the exact classical and quantum mechanical descriptions of the time evolution of a metastable configuration of particles, e.g., unimolecular fragmentation. Of course, the general metastable system, with N particles and nonlinear interactions, is too complex to permit much progress to be made towards finding exact relationships between features of its classical and quantum mechanical descriptions. Nevertheless, the success of recent adaptations and extensions of the theory of classical Hamiltonian mappings[1,2] in the analysis of vibrational energy exchange[3] and unimolecular reaction[4–6] stimulates our interest in formulating the analogous quantum mechanical analyses. Given that the classical mechanical theory makes extensive use of the properties of trajectories, the extension to quantum theory is not obvious.

We have chosen, as a vehicle for our study, the scattering of a point particle from three hard circular discs in a plane,[7] which shares with many other scattering problems[8] the feature of irregular scattering, i.e., a clustering of initial conditions that lead to delayed trajectories, including a set with measure zero that lead to asymptotic ($t \to \infty$) trapping in the interaction region. The quantum mechanical description of this scattering problem is expected to have resonances, and we seek to correlate these resonances with properties of the delayed trajectories. The rate of leakage of a delayed trajectory from the interaction region is our analog to the rate of decay of a metastable system and our doorway to a better understanding of the quantum mechanics of a classically chaotic metastable system.

One of the motivations for the work reported in this and the following papers is the need to develop a quantum mechanical version of the improved theory of the rate of unimolecular reaction proposed by Gray and Davis,[4] and Gray, Rice, and Davis.[5] In that theory, which is based on classical mechanics, the bottlenecks to intramolecular energy redistribution and to fragmentation are separately identified. The former bottleneck is associated with the several cantori that bound the regions of quasiperiodic motion and the latter bottleneck with the separatrix of the system. With the assumption that the rates of crossing of these bottlenecks are independent, and that the separatrix is the surface defining the transition state, this modified statistical theory gives an excellent description of the rates of unimolecular reactions even for systems which are very badly described by RRKM theory.

As already mentioned, the extensive use of the properties of trajectories in the theory just described makes it difficult to develop a quantum mechanical version of the theory. The general idea which we seek to exploit is that there exist universal relationships between the classical trajectories and the quantum mechanical resonances associated with a classical repellor (see the following paper).

We expect the phase space of a typical Hamiltonian system, such as a set of coupled nonlinear oscillators, to decompose into several invariant sets among which there are: (i) the set of trajectories coming from and escaping to infinity; (ii) a hierarchy of Cantori which form partial barriers to escaping; (iii) a hierarchy of bounded quasiperiodic motions which form complete barriers to escaping. The set of trajectories which are bounded, including (ii) and (iii), form the classical repellor for the set (i) of unbounded trajectories. This complex trajectory structure is only partially understood. The origin of most difficulties is the fact that a typical Hamiltonian dynamics is both focusing and defocusing. Focusing of trajectories causes quasiperiodic islands to appear in the Poincaré surface of section, whereupon stable periodic orbits are mixed in a complex manner with unstable periodic orbits. Focusing of trajectories also generates caustics, which require careful treatment when the system dynamics is quantized. The dynamics of the class of mechanical systems which are everywhere defocusing is much better understood than is the dynamics of general systems. For the everywhere defocusing systems, the phase space is expected to decompose in a simple way into: (i) the set of trajectories coming from and escaping to infinity; (ii) one or several transitive invariant sets of completely unstable trajectories forming the classical repellor. No stable periodic orbits exist in this class of systems.

 0021-9606/89/042225-17$02.10

In this series of papers we shall construct a quantum theory of the escape rate for mechanical systems whose classical dynamics is everywhere defocusing, even when the classical repellor is chaotic. Indeed, in the following paper we shall show, in the semiclassical limit, that classical chaos allows some quantum scattering resonances to have lifetimes longer than the classical lifetimes, which we believe is the first demonstration of a direct effect of classical chaos on a quantum property. As already mentioned, the vehicle for executing this program is the study of the scattering of a point particle from three hard discs in a plane. This paper describes the classical mechanics of that system, the following paper describes a semiclassical treatment of the scattering resonances and their relationships with trajectories, and the paper following that describes the complete analysis of the quantum mechanics of scattering of a point particle from three hard discs in a plane.

II. BACKGROUND

It is now well established that a generic classical bounded Hamiltonian system exhibits both regular and chaotic dynamics.[9] The source of the chaotic dynamics is generally associated with nonlinear terms in the Hamiltonian leading to an extraordinary sensitivity of the dynamics to initial conditions. The characteristic feature of the chaotic dynamics is a measure preserving ergodic (or possibly mixing) flow with positive Kolmogorov–Sinai entropy. In general, the system phase space (e.g., as visualized in a Poincaré surface of section) has islands where trajectories are bounded by a quasi-periodic torus, embedded in a sea of trajectories where the motion is chaotic.[10] In contrast, a generic quantum mechanical bounded Hamiltonian system has a discrete spectrum of eigenstates, hence the expectation value of any observable evolves in time as an almost-periodic function, which is known to be recurrent, so that no mixing occurs.[11] Furthermore, the Kolmogorov–Sinai entropy is zero,[12] and there is no possibility for chaos of the type described for the classical dynamics of the same system.

We are concerned with the description of the dynamics of unbounded systems, for which the fundamental theory is incompletely developed. Taking as our lead the success of "billiard"[13] and "stadium"[14] models in the illustration of the features of completely chaotic bounded trajectories,[15] we examine the scattering of a point particle from three hard discs fixed in a plane. Most of our results focus on the special case when the discs are located at the vertices of an equilateral triangle, but some are more general. We take the disc radius to be $a = 1$ and the center-to-center separation (length of the side of the triangle) to be R. The phase space of the system is the real space $\{(x,y,v_x,v_y)\}$ outside of the discs, $(x-x_i)^2 + (y-y_i)^2 \leqslant a^2$, where (x_i,y_i) are the centers of the discs (see Fig. 1). This phase space is stratified into subspaces of constant energy, $\{(x,y,\theta)\}$, where θ is the polar angle of the velocity vector ($v_x = v\cos\theta$, $v_y = v\sin\theta$).

A. The classical repellor (Ω_R)

Consider, first, the scattering of a point particle from two hard discs fixed in a plane. There is a unique unstable periodic trajectory trapped by repeated collisions between the discs. The trajectory is obviously unstable since a small displacement leads to defocusing on reflection from the curved surface of a disc. This unique trajectory is called a repellor, denoted Ω_R. The dimension of the repellor is one, and the escape rate (γ) from the trapped configuration is equal to the rate of separation of the particular trajectory from the periodic trajectory, defined by its Lyapunov exponent (λ_1). As the dynamics on the repellor is regular, the Kolmogorov–Sinai entropy of the system is zero. The S matrix for this system is known to have resonances.[18]

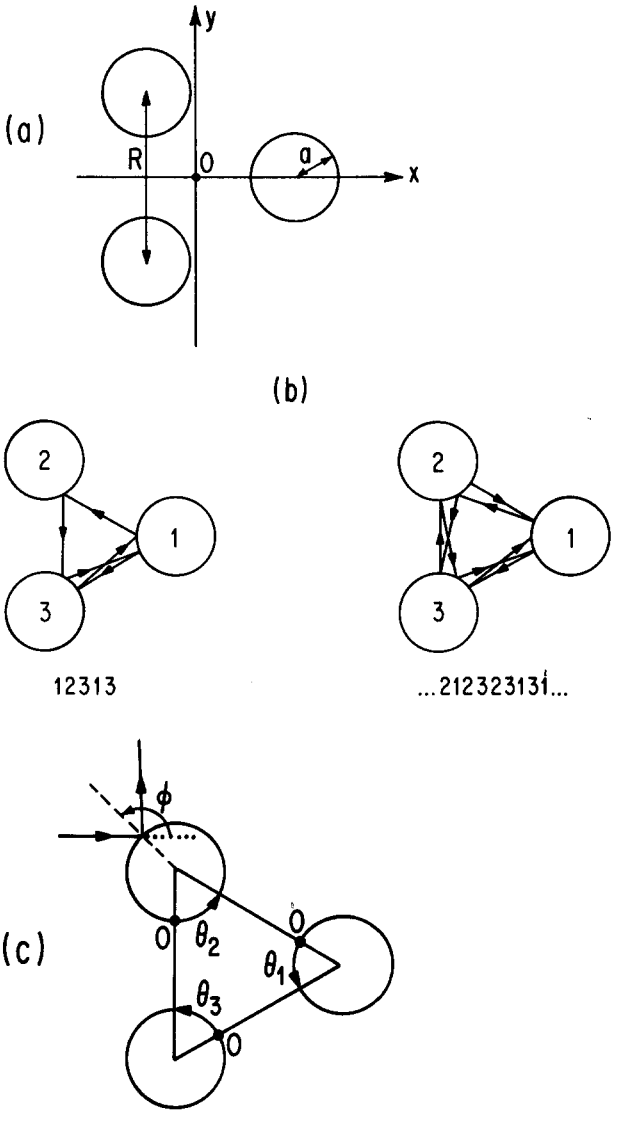

FIG. 1. (a) The geometry of the system. The three hard discs are fixed in the plane at the vertices of an equilateral triangle with side R. The radius of a disc is a. (b) Two examples of trajectories of the repellor: the periodic trajectory 12313 and the trajectory ...212323131... . (c) The coordinates of the impact points and of the incident ray on the discs.

Consider now the scattering of a point from three or more discs fixed in the plane. In general, we expect there to be a set of trajectories which are trapped in the scattering region, i.e., remain confined to the scattering region as $t \to \infty$. This set of trajectories is the repellor Ω_R for the system. Note that the trajectories that constitute Ω_R have positive energies, so that Ω_R does not contain the bound states of the

system. In general, Ω_R may be a simple set containing a finite or countably infinite number of periodic trajectories, or it may be a Cantor set. For the conservative Hamiltonian system we are interested in, all the trajectories of Ω_R are of the saddle type, in one-to-one correspondence with doubly infinite sequences of the symbols {1,2,3},

$$\mathbf{s} = \cdots s_{-2}s_{-1}s_0s_1s_2\cdots, \tag{2.1}$$

with the only constraint $s_{n+1} \neq s_n$ under certain conditions (see Sec. III). The symbol s_n is the label of the disc involved in the nth collision.[7] The set of all sequences $\mathbf{s}$ is called a symbolic dynamics.[9,19] The trajectories which only stay for a finite time in the trapping region are represented by finite strings of symbols and are outside the symbolic dynamics of the repellor Ω_R. Moreover, there are both stable, $W^s(\Omega_R)$. and unstable, $W^u(\Omega_R)$, manifolds of trajectories associated with Ω_R.[9,19]

The repellor Ω_R and the natural measure it supports are characterized by several quantities, which we now describe.

B. The Lyapunov exponents (λ_i)[19,20]

These are defined by the rate of separation of initially infinitesimally displaced trajectories. For a system with f degrees of freedom two of the Lyapunov exponents are zero by virtue of (i) energy conservation and (ii) lack of separation of trajectories along the direction of flow of the trajectories. The reversibility of the equations of motion implies that there are $f-1$ positive or zero Lyapunov exponents and $f-1$ negative or zero Lyapunov exponents:

$$\lambda_1 \geqslant \lambda_2 \geqslant \cdots \geqslant \lambda_{f-1} \geqslant 0 \geqslant \lambda_f \geqslant \lambda_{f+1} \geqslant \cdots \geqslant \lambda_{2f-2}. \tag{2.2}$$

For a system described by a conservative Hamiltonian, as in our case, Liouville's theorem imposes the constraint of conservation of phase space density, which implies that

$$\sum_{i=1}^{2f-2} \lambda_i = 0. \tag{2.3}$$

In our case $f=2$, hence Eq. (2.3) implies that

$$\lambda_1 > 0 > \lambda_2 = -\lambda_1. \tag{2.4}$$

C. The Kolmogorov–Sinai entropy per unit time (h_{KS})[9,19]

This important quantity measures the rate of accumulation of data necessary to follow, without ambiguity, a trajectory *on* the repellor. If the sampling rate is smaller than h_{KS}, then a long observation will yield a set of trajectories rather than a single trajectory. When h_{KS} is positive the system is chaotic and the average number of symbols necessary to reconstruct the repellor Ω_R from the symbolic dynamics of sequences is $E^{h_{KS}\Delta t}$, where Δt is the time interval between samplings.[21]

D. The Hausdorff dimension (D_H)[22,23]

This quantity is the most dramatic characterization of the repellor Ω_R. When Ω_R fills almost completely a domain of the phase space, D_H is close to the dimension of the phase space, namely $2f-1$. However, if Ω_R is filamentary, D_H is close to one. Thus, comparing Ω_R to a sponge with holes on all size scales, the Hausdorff dimension is a measure of the "bulkiness" of the repellor. If a Poincaré surface of section[9] is used to represent the motion in Ω_R, the dimension of that Poincaré surface of section is $D_H - 1$. In a system with f degrees of freedom the dimension of a local stable manifold, or of a local unstable manifold, is f. Then the intersection of the unstable manifold with the Poincaré surface of section is a Cantor set of Hausdorff dimension

$$d_H \equiv \tfrac{1}{2}(D_H - 1), \tag{2.5}$$

composed of local unstable manifolds of dimension $f-1$.

E. The information dimension (D_I)[19,33]

In contrast with the Hausdorff dimension which characterizes the bulkiness of the invariant set Ω_R itself, the information dimension characterizes the bulkiness of the invariant probability measure built upon Ω_R. We expect both dimensions to be similar. In general, they satisfy the inequality[33]

$$D_I \leqslant D_H. \tag{2.6}$$

The information dimension is important because it is given in terms of the Lyapunov exponents and the entropy per unit time by the following relation valid for a two-dimensional system[19,23]:

$$D_I = h_{KS}\left(\frac{1}{\lambda_1} + \frac{1}{|\lambda_2|}\right) + 1. \tag{2.7}$$

Since $\lambda_2 = -\lambda_1$ for a Hamiltonian system [see Eq. (2.4)],

$$D_I = \frac{2h_{KS}}{\lambda_1} + 1. \tag{2.8}$$

The information dimension for the unstable manifold can be defined in analogy with Eq. (2.5), whereupon

$$d_I = \frac{h_{KS}}{\lambda_1}. \tag{2.9}$$

Note that when $h_{KS} > 0$, D_I may be a noninteger dimension.

F. The escape rate (γ)[19,24–26]

This quantity is the conventional characterization of the repellor. Imagine that Ω_R is enclosed in a large box B $\{x^2 + y^2 < b^2, (v_x, v_y)$ arbitrary$\}$ with $b \gg R$ and a. Suppose N_0 scattering experiments are carried out. In each such experiment the incident energy of the point particle, hence its speed, is taken to be the same, but the incident directions are different. We seek to determine the fraction of scattering trajectories delayed long enough that at time t the point particle remains inside B. In general we expect this fraction, N_t/N_0, to decay with increasing t either as an exponential or as a power law:

$$\frac{N_t}{N_0} \simeq C(E)e^{-\gamma(E)t} \tag{2.10}$$

or[16,17]

$$\frac{N_t}{N_0} \simeq C(E)t^{-\zeta(E)}. \tag{2.11}$$

For the case we study in this paper we expect Eq. (2.10) to hold, whereupon the escape rate $\gamma(E)$ is given by[19,24,26]

$$\gamma(E) = \sum_{\lambda_i > 0} \lambda_i(E) - h_{KS}(E). \quad (2.12)$$

The time dependence shown by Eq. (2.11) is expected to hold for two-dimensional Hamiltonian systems with quasi-periodic islands (see Ref. 15).

The interpretation of Eq. (2.12) is as follows.[24,26] A cell in phase space is expanded by the flow at a rate $\Sigma_{\lambda_i>0}\lambda_i(E)$. This expansion has two effects: it generates, via diverging trajectories, randomization on the repellor described by $h_{KS}(E)$, and it also generates a nonzero rate of escape from the repellor, $\gamma(E)$. Note that the randomization of the trajectories acts as an inhibitor to escape from Ω_R. When the ensemble of point particle scattering experiments includes dispersion in the incident energy, consideration must be given to effects which arise near zero energy, as discussed in Appendix A.

In our two-dimensional scattering problem the escape rate at fixed energy can be expressed in terms of the information dimension of the repellor, using Eq. (2.8), in the form

$$\gamma(E) = \tfrac{1}{2}\lambda_1(E)[3 - D_I(E)], \quad 1 \leqslant D_I(E) \leqslant 3. \quad (2.13)$$

We note that the escape rate is zero when the repellor fills the whole phase space since then $D_I(E) = 3$. Thus, the information dimension can also be used as a characterization of the rate of escape from the repellor. For the system we study here, the dependence on energy of the various quantities described above is very simple, namely

$$\gamma(E) = v\tilde{\gamma}, \lambda_1(E) = v\tilde{\lambda}_1, \quad h_{KS}(E) = v\tilde{h}_{KS}, \quad (2.14)$$

where $v = (2E/m)^{1/2}$ is the velocity of the particle and $\tilde{\gamma}, \tilde{\lambda}_1$, and $\tilde{h}_{KS}$ are defined per unit length of trajectory.

G. The time delay function[8]

The details of the escape of the scattered point particle from Ω_R are contained in a time delay function defined as follows. Let an incoming point particle trajectory cross the boundary ∂B of B at t_0 and exit at t_1. If the system has f degrees of freedom $2f-1$ initial conditions on ∂B uniquely characterize the trajectory. The time delay function, denoted $T(X_0)$, is the mapping from this $(2f-1)$ dimensional space of initial conditions X_0 on ∂B to the time elapsed inside $B (T = t_1 - t_0)$.

Although we expect almost all point particles to escape from B, there will be some initial conditions X_0 which belong to the stable manifold $W^s(\Omega_R)$, in which case $t_1 \to \infty$ and the trajectory of the particle remains in Ω_R forever. Thus, the time delay function is singular on the stable manifold $W^s(\Omega_R) \cap \partial B$. In the case of scattering of a point particle by three discs, $f = 2$ and the dimension of the boundary of B is 3. Then the repellor is a Cantor set, leading to a very complex time delay function such as shown in Figs. 2 and 3.

These two examples (Figs. 2 and 3) of time delay functions were obtained by constructing numerically the trajectory for various initial conditions. The enlargement of the time delay function shows its self-similar geometry, which is governed by a doubling of the number of peaks when the time delay increases, as observed in Fig. 3 for $R = 3.5$. In Fig. 2 for $R = 2.5$, the rightmost structure is more complicated because of multiple impacts between discs 2 and 3 for initial conditions $0.25 < y_0 < 0.5$, before entering the trapping region. In Fig. 3, the first impact is always on disc 1 for all the initial conditions displayed.

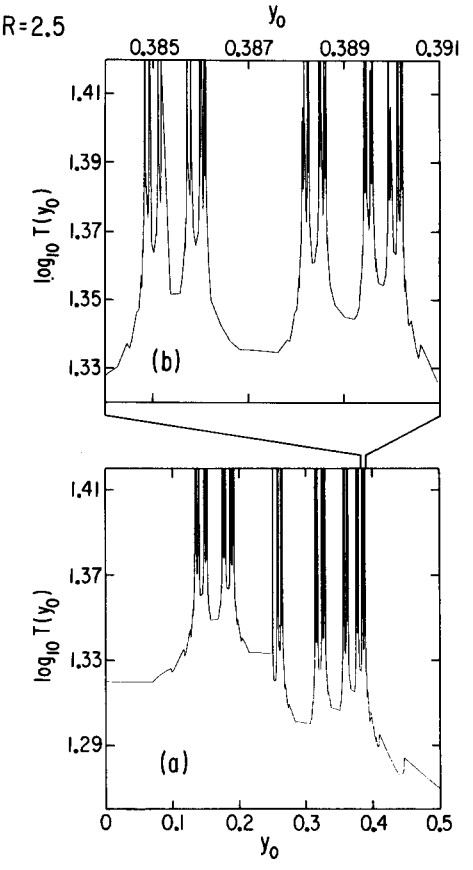

FIG. 2. (a) The time delay function $T(y_0)$ of the three hard disc system when $R = 2.5$ and $v = 1$. The initial conditions are $x_0 = -10, 0 < y_0 < 0.5$, and $\theta_0 = 0$. The ball B enclosing the repellor has a radius $b = 10$. $\log_{10} T(y_0)$ is plotted vs y_0. The discontinuities in the slope at the bottom of the time delay function occur when the trajectory becomes tangent to one of the discs. Then the history of the trajectory is modified discontinuously but the time delay remains continuous. However, the time delay function is singular and infinite when the initial condition y_0 belongs to the fractal stable manifold of the repellor. (b) Enlargement of the time delay function showing its self-similar geometry.

Now, the number of scattering events that leave the point particle in B at t is

$$\frac{N_t}{N_0} \simeq \nu\{X_0 : T(X_0) > t\}, \quad (2.15)$$

where ν is the measure representing the ensemble of N_0 point particles. The measure ν is absolutely continuous with respect to the Riemann measure on ∂B. The set of singularities of the time delay function has a Hausdorff dimension $\tilde{d}_H \leqslant 2f-1$, given by $\tilde{d}_H = d_H + 2$, when $f = 2$. The number of balls of diameter ϵ necessary to cover the entire set is

$$M(\epsilon) \sim \epsilon^{-\tilde{d}_H}. \quad (2.16)$$

Let $\epsilon(t)$ be the smallest possible diameter of the balls in a covering of the set $\{X_0 : T(X_0) > t\}$. Then

$$\nu\{X_0 : T(X_0) > t\} \sim \epsilon^{2f-1} M(\epsilon) \sim \epsilon\,(t)^{2f-1-\tilde{d}_H}. \quad (2.17)$$

If the decay of N_t is exponential

$$\epsilon(t) \sim e^{-\gamma(E)t/(2f-1-\tilde{d}_H)}, \quad (2.18)$$

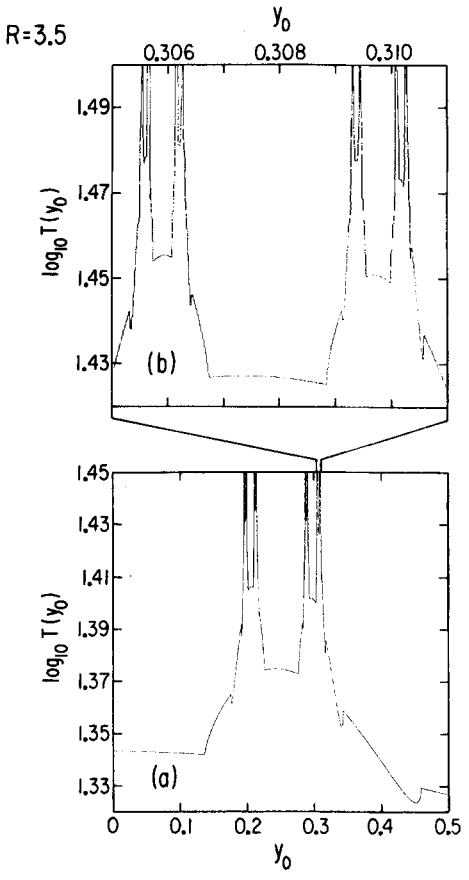

FIG. 3. (a) The time delay function $T(y_0)$ when $R = 3.5$ for the same initial conditions and ball B as in Fig. 2. (b) Enlargement of the time delay function showing its self-similar geometry.

whereas if the decay of N_t follows a power law[16,17]

$$\epsilon(t) \sim t^{-\zeta(E)/(2f-1-\tilde{d}_H)}. \tag{2.19}$$

Thus, the properties of the trajectories that escape from B can be characterized by a combination of the fractal properties of the singularities of the time delay function. We expect, for the scattering of a point particle by discs on the plane, a scaling of the time delay function with energy of the form

$$T(X_{01},X_{02},E) = (m/2E)^{1/2} L(X_{01},X_{02}). \tag{2.20}$$

III. CONSTRUCTION OF THE PARTITION OF PHASE SPACE AND THE SYMBOLIC DYNAMICS

To construct the invariant measure of the classical repellor we first construct a partition of the phase space which clearly relates the coding of the trajectories with the sequence of collisions with the discs. The coordinates of the points of impact of the particle on the perimeters of the discs will be denoted θ_1, θ_2, or θ_3, respectively. In addition, let ϕ be the angle between a unit vector normal to the disc and the unit vector along an incident trajectory (see Fig. 1). The phase space of the three disc system is then composed of three rectangles (see Fig. 4). Clearly, in order to describe the repellor composed of trajectories which stay trapped between the discs we need only consider the angles $0 \leqslant \theta_1 \leqslant \pi/3$, $0 \leqslant \theta_2 \leqslant \pi/3$, $0 \leqslant \theta_3 \leqslant \pi/3$. Indeed, the trajectories with θ_i outside these domains will escape.

We define the cell of disc 1 to consist of trajectories which will hit disc 2 in the domain $0 \leqslant \theta_2 \leqslant \pi/3$. We call this cell $\cdot 12$, the dot labeling the initial time. The image of $\cdot 12$ by the flow is the cell $1 \cdot 2$, obtained by shifting to the left the integers with respect to the dot. We call σ such a shift. The cell $\cdot 12$ is bounded by two curves: $\phi = \phi_0(\theta_1)$ and $\phi = \phi_1(\theta_1)$, where $\phi_0(\theta_1)$ is the set of points mapped onto $\theta_2 = \pi/3$ by the flow, and $\phi_1(\theta_1)$ is the set of points mapped onto $\theta_2 = 0$. Some geometry shows that

$$\phi_0(\theta) = \pi + \operatorname{arctg}\left(\frac{\sin\theta}{\cos\theta - a/(R-a)}\right), \tag{3.1}$$

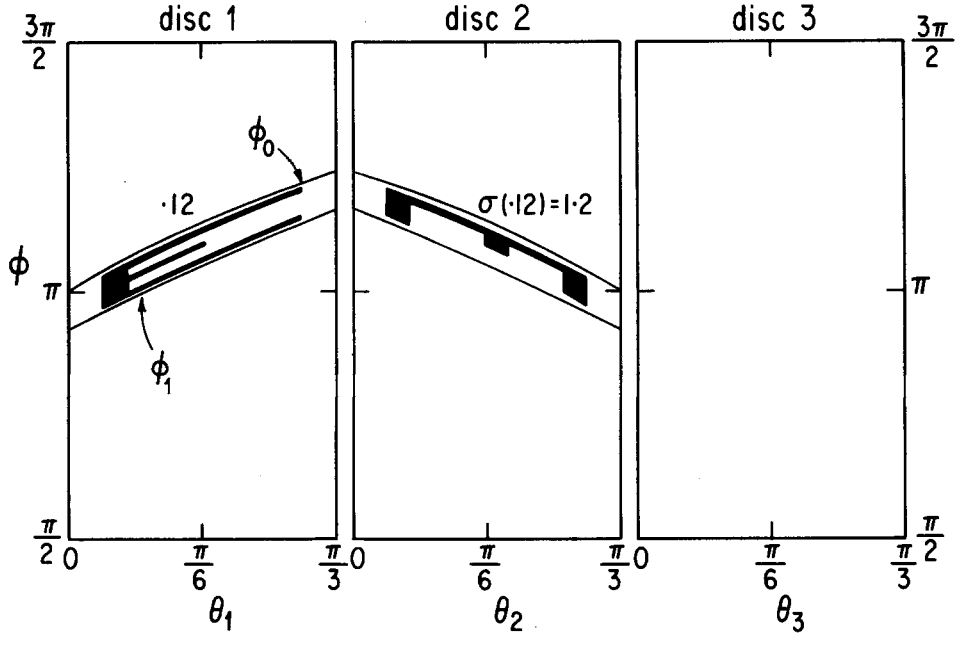

FIG. 4. Phase space of the 3 disc system, represented by the set of impact points (θ_1, θ_2, θ_3) and incident angles ϕ. The cell $\cdot 12$ is the set of initial conditions on disc 1 mapped onto disc 2 on the points $0 < \theta_2 < \pi/3$ at the next collision. Its image is the cell $1 \cdot 2$. The image of the E shows how the cell is stretched by the dynamics.

$$\phi_1(\theta) = \pi + \text{arctg}\left(\frac{\sin\theta - 3^{1/2}a\cos\theta/(2R-a)}{\cos\theta + 3^{1/2}a\sin\theta/(2R-a) - 2a/(2R-a)}\right). \tag{3.2}$$

The small sides of the cell have a length

$$\Delta\phi(0) \equiv \phi_0(0) - \phi_1(0) = \Delta\phi(\pi/3) = \text{arctg}\left(\frac{3^{1/2}a}{2R-3a}\right). \tag{3.3}$$

When the distance R between the centers of the discs is large,

$$\phi_0(\theta) = \pi + \theta + \frac{a}{R}\sin\theta + O(a^2/R^2), \tag{3.4}$$

$$\phi_1(\theta) = \pi + \theta + \frac{a}{R}(\sin\theta - 3^{1/2}/2) + O(a^2/R^2), \tag{3.5}$$

$$\Delta\phi(0) = \Delta\phi(\pi/3) = \frac{3^{1/2}a}{2R} + O(a^2/R^2). \tag{3.6}$$

We obtain the boundary of $1\cdot 2 = \sigma(\cdot 12)$ by inversion around $\theta_2 = \pi/6$.

Similarly, we can obtain the cell $\cdot 13$ by inversion around $\theta_1 = \pi/6$ following by another inversion around $\phi = \pi$. The cells $\cdot s_0 s_1$ and $s_{-1}\cdot s_0$ are obtained by permutation of the coordinates (see Fig. 5). The intersections of the cells $\cdot s_0 s_1$ with the cells $s_{-1}\cdot s_0$ define 12 cells $s_{-1}\cdot s_0 s_1$, as shown in Fig. 6. The classical repellor is necessarily contained in these 12 cells.

The repellor is obtained by iterating the above procedure, which generates finer and finer cells, denoted

$$s_{-m}s_{-m+1}\cdots s_{-1}\cdot s_0 s_1\cdots s_n, \tag{3.7}$$

or equivalently $\Delta_m^n(\mathbf{s})$, where $\mathbf{s}$ is a bi-infinite sequence of symbols $\{1,2,3\}$

$$\mathbf{s} = \cdots s_{-2}s_{-1}\cdot s_0 s_1 s_2\cdots. \tag{3.8}$$

All these cells are contained within each other in the sense

$$\Delta_{-m}^{n}(\mathbf{s}) \subset \Delta_{-m'}^{n'}(\mathbf{s}) \quad \text{if } -m < -m' \text{ and } n' < n. \tag{3.9}$$

In the limit $m,n \to \infty$, the classical repellor is obtained as the set of points in correspondence with the bi-infinite sequences $\mathbf{s}$. We observe that in such a sequence doublets such as 11, 22, or 33 do not occur, which is equivalent to the constraint $s_{n+1} \neq s_n$. This constraint is also implicit in the topological transition matrix (whose matrix elements describe allowed successive collision paths)

$$\chi = \begin{bmatrix} 0 & 1 & 1 \\ 1 & 0 & 1 \\ 1 & 1 & 0 \end{bmatrix}. \tag{3.10}$$

The number of admissible doublets is then 6, of triplets is 12, etc. The number of cells obtained after n iterations (including all the previous ones) grows as

$$e^{h_{\text{top}}n}, \tag{3.11}$$

where $h_{\text{top}} = \ln 2$ is the topological entropy of the system. h_{top} is given by the logarithm of the largest eigenvalue of χ.[32]

We observe that the geometric construction of the partition of phase space and the abovementioned properties are valid only for R large enough. As R decreases from infinity the curves ϕ_0 and ϕ_1 reach the values $\phi = \pi/2$ and $\phi = 3\pi/2$. Then the boundaries of the cells contain some trajectories *tangent* to the discs and the partitioning of the phase space becomes more complicated. We note that the Markovian partition of phase constructed by Bunimovich and Sinai[13] for the three disc bounded case $R = 2a$ is composed of a countable number of symbols, which shows how complicated the situation becomes as $R \to 2a$. In our treatment we shall assume $R > 3a$, a condition which is sufficient for the above symbolic dynamics to hold on $\{1,2,3\}$ with the topological transition matrix χ given in Eq. (3.10). This symbolic dynamics, which we denote (S,σ) is composed of the shift σ

$$(\sigma\mathbf{s})_n = \mathbf{s}_{n+1} \tag{3.12}$$

acting on the set

$$S = \{\mathbf{s} = \cdots s_{-2}s_{-1}\cdot s_0 s_1 s_2\cdots : \chi_{s_n s_{n+1}} = 1\}. \tag{3.13}$$

The symbolic dynamics is called a topological Markov chain with transition matrix χ.[32] The above construction shows that there exists a one-to-one correspondence J between the sequence $\mathbf{s}$ of S and the points of the repellor on the discs:

$$J(\mathbf{s}) = X(0), \tag{3.14}$$

where $X(0)$ is a point on the circumference of a disc at time 0.

Now let us consider a trajectory $X(t)$ of the repellor. The times of intersection with the circumferences of the discs are the following:

$$\cdots < t_{-2} < t_{-1} < t_0 < t_1 < t_2 < \cdots.$$

If Φ^t denotes the flow, we have

$$\Phi^{t-t_0}X(t_0) = X(t) \quad \text{for} \quad t_0 \leqslant t \leqslant t_1, \tag{3.15}$$

so that a point belonging to the repellor is associated with both a sequence $\mathbf{s}$ and the time τ elapsed since the previous impact, i.e.,

$$\Phi^t[\mathbf{s},\tau] = [\mathbf{s},\tau + t] \quad \text{if} \quad 0 \leqslant \tau, \tau + t < T(\mathbf{s}), \tag{3.16}$$

where $T(\mathbf{s})$ is here the time of flight between the points $J(\mathbf{s})$ and $J(\sigma\mathbf{s})$:

$$\Phi^{T(\mathbf{s})}J(\mathbf{s}) = J(\sigma\mathbf{s}). \tag{3.17}$$

We identify

$$[\mathbf{s},T(\mathbf{s})] = [\sigma\mathbf{s},0]. \tag{3.18}$$

For an arbitrary time t we have

$$\Phi^t[\mathbf{s},\tau] = [\sigma^k\mathbf{s},\tau^* = t + \tau - T(\mathbf{s}) - T(\sigma\mathbf{s}) - \cdots - T(\sigma^{k-1}\mathbf{s})] \tag{3.19}$$

if the time τ^* is between 0 and $T(\mathbf{s})$. We shall denote by F the space of all possible values of $[\mathbf{s},\tau]$, i.e.,

$$F = \{[\mathbf{s},\tau] : \mathbf{s} \in S, \quad 0 \leqslant \tau < T(\mathbf{s})\}. \tag{3.20}$$

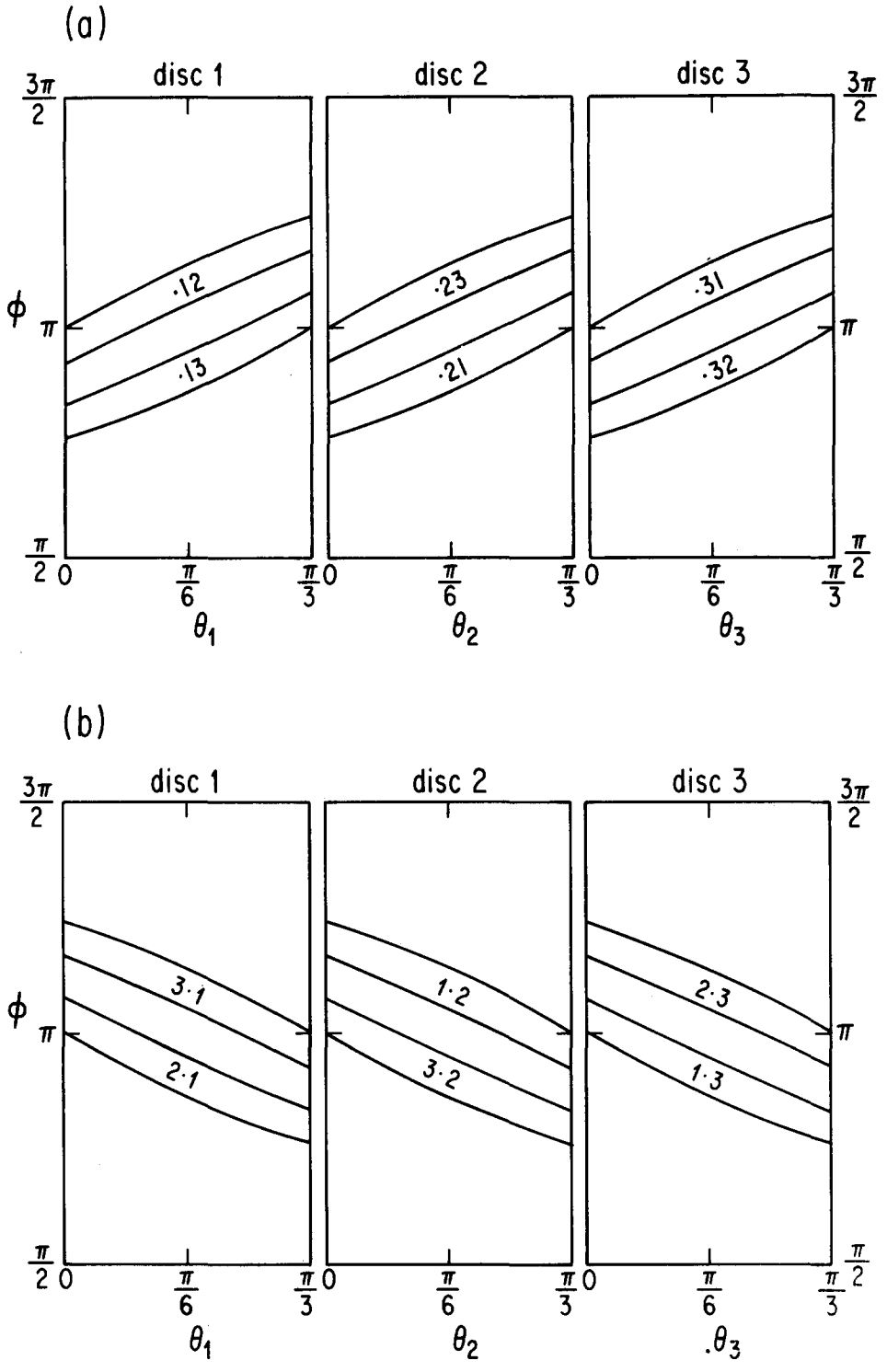

FIG. 5. (a) The partition of the repellor into six two-symbol cells in the phase space of Fig. 4, when $R = 3.2$. (b) The images of these six cells.

IV. CONSTRUCTION OF THE NATURAL INVARIANT MEASURE

A. The local Lyapunov number

This invariant measure μ is defined by the trajectories which are trapped inside the repellor. Clearly, the space sampled by these trajectories depends on the local defocusing $\kappa^{(u)}(X)$, where $\kappa^{(u)}(X)$ is the curvature of the unstable manifold at point X of the repellor. If the impact times and the angles between the incident trajectory and the exterior normal at the impact points are

$$\cdots t_{-5}t_{-4}t_{-3}t_{-2}t_{-1}t_0,$$

$$\cdots \phi_{-5}\phi_{-4}\phi_{-3}\phi_{-2}\phi_{-1}\phi_0, \quad \frac{\pi}{2} \leqslant \phi_i \leqslant \frac{3\pi}{2},$$

and if we define $\tau_{-n} = t_{-n+1} - t_{-n} > 0$, the curvature $\kappa^{(u)}(X)$ is given by the continued fraction[13,14]

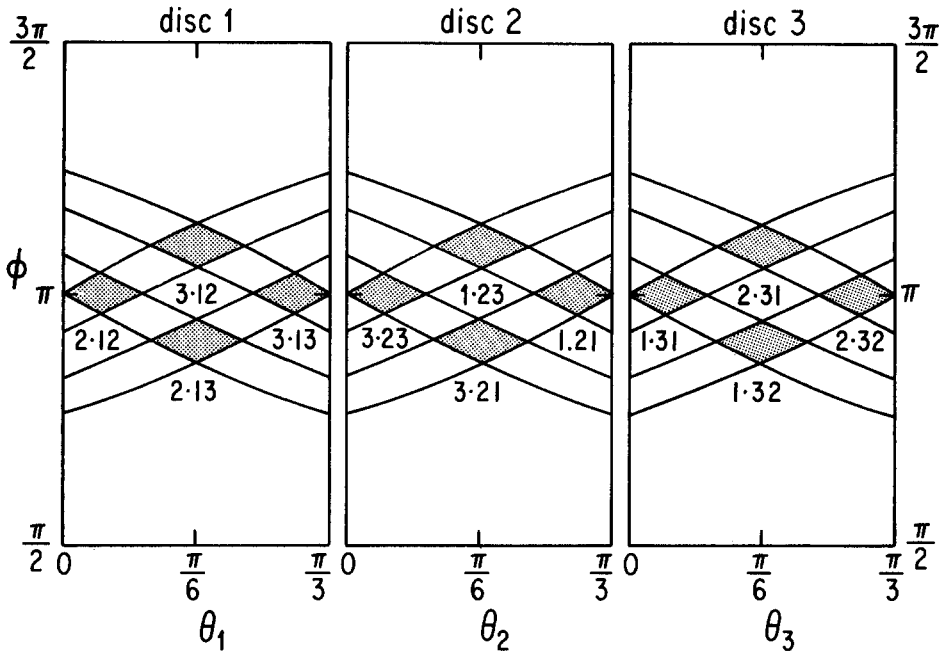

FIG. 6. The partition of the repellor into the 12 three-symbol cells defined by the intersection of Figs. 5(a) and 5(b), when $R = 3.2$.

$$\kappa^{(u)}(X) = \cfrac{1}{\tau_{-1} + \cfrac{1}{-\cfrac{2v}{a\cos\phi_{-1}} + \cfrac{1}{\tau_{-2} + \cfrac{1}{-\cfrac{2v}{a\cos\phi_{-2}} + \cfrac{1}{\tau_{-3} + \cdots}}}}}. \tag{4.1}$$

$\kappa^{(u)}(X)$ is positive because $\cos\phi_{-i} < 0$. The Lyapunov exponent over the natural invariant measure μ is then

$$\lambda_1 = \int \kappa^{(u)}(X)\mu(dX) = \lim_{t\to\infty} \frac{1}{t}\int_0^t \kappa^{(u)}[X(\tau)]d\tau. \tag{4.2}$$

μ is a singular measure with respect to the Lebesgue measure. To obtain the factor by which the cells of a partition are stretched by the flow over a finite time, we need to integrate $\kappa^{(u)}[X(t)]$ over this time and then exponentiate the result. We obtain then what we shall call the local Lyapunov number from point $\mathbf{s}$ to point $\sigma\mathbf{s}$:

$$\Lambda_{\mathbf{s}} = \exp\left[\int_{t_{\mathbf{s}}}^{t_{\sigma\mathbf{s}}} \kappa^{(u)}[X(t)]dt\right] > 1, \tag{4.3}$$

where the trajectory goes from $X(t_{\mathbf{s}}) = J(\mathbf{s})$ to $X(t_{\sigma\mathbf{s}}) = J(\sigma\mathbf{s})$. Integrating, we obtain

$$\Lambda_{\mathbf{s}} = \frac{2l_{\mathbf{s},\sigma\mathbf{s}}}{a|\cos\phi_{\mathbf{s}}|} + 1 + \cfrac{t_{\sigma\mathbf{s}} - t_{\mathbf{s}}}{t_{\mathbf{s}} - t_{\sigma^{-1}\mathbf{s}} + \cfrac{1}{-\cfrac{2v}{a\cos\phi_{\sigma^{-1}\mathbf{s}}} + \cdots}}, \tag{4.4}$$

with the definition $l_{\mathbf{s},\sigma\mathbf{s}} \equiv \mathrm{dist}(\mathbf{s},\sigma\mathbf{s}) \equiv v(t_{\sigma\mathbf{s}} - t_{\mathbf{s}})$.

In what follows we shall only need to approximate values of $\Lambda_{\mathbf{s}}$ for any point $\mathbf{s}$ in a given domain $\mathbf{a}$. The image of $\mathbf{a}$ is chosen as $\mathbf{b}$, corresponding to $\sigma\mathbf{s}$. We choose

$$\mathbf{a} = S_{-n/2}\cdots S_{-2}S_{-1}\cdot S_0 S_1\cdots S_{(n/2)-1}, \quad n \text{ even},$$
$$\mathbf{b} = S_{-(n/2)+1}\cdots S_{-1}S_0\cdot S_1 S_2\cdots S_{n/2}, \tag{4.5}$$
$$\mathbf{a} = S_{(-n+1)/2}\cdots S_{-2}S_{-1}\cdot S_0 S_1\cdots S_{(n-1)/2}, \quad n \text{ odd},$$
$$\mathbf{b} = S_{(-n+3)/2}\cdots S_{-1}S_0\cdot S_1 S_2\cdots S_{(n+1)/2}. \tag{4.6}$$

Then we take

$$\Lambda_{\mathbf{ab}}^{(n)} = \min_{\substack{\mathbf{s}\in\mathbf{a}\\ \sigma\mathbf{s}\in\mathbf{b}}} \Lambda_{\mathbf{s}} \quad \text{or equivalently} \quad \max_{\substack{\mathbf{s}\in\mathbf{a}\\ \sigma\mathbf{s}\in\mathbf{b}}} \Lambda_{\mathbf{s}}. \tag{4.7}$$

We observe that for R large enough,

$$\Lambda_{\mathbf{ab}}^{(n)} = \frac{2R}{a|\cos\phi_{\mathbf{a}}^{(n)}|} + O(1). \tag{4.8}$$

Similarly, we define

$$l_{\mathbf{ab}}^{(n)} = \min_{\substack{\mathbf{s}\in\mathbf{a}\\ \sigma\mathbf{s}\in\mathbf{b}}} \mathrm{dist}(\mathbf{s},\sigma\mathbf{s}) \quad \text{or equivalently} \quad \max_{\substack{\mathbf{s}\in\mathbf{a}\\ \sigma\mathbf{s}\in\mathbf{b}}} \mathrm{dist}(\mathbf{s},\sigma\mathbf{s}). \tag{4.9}$$

We now calculate $\Lambda_{\mathbf{ab}}^{(n)}$ when $n = 2$ and $n = 3$.

(i) Order $n = 2$: There are two different cases to consider (see Fig. 7). We observe that at order $n = 2$, the distances $l_{\mathbf{ab}}^{(n)}$ can not be defined to order $O(a)$ for large R, so that

$$l_{\mathbf{ab}}^{(2)} = R \tag{4.10}$$

in this approximation. Similarly $\Lambda_{\mathbf{ab}}^{(2)}$ is not defined to order $O(1)$ so that

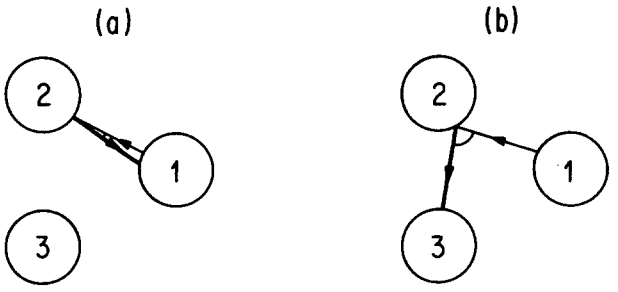

FIG. 7. Examples of the two different cases of flights at the $n=2$ approximation: (a) flight $1\cdot2\to2\cdot1$ and (b) flight $1\cdot2\to2\cdot3$.

$$\Lambda_{ab}^{(2)}=\frac{2R}{a} \quad \text{for} \quad \{1\cdot2\to2\cdot1,\cdots\} \quad \text{and}$$

$$\frac{4R}{3^{1/2}a} \quad \text{for} \quad \{1\cdot2\to2\cdot3,\cdots\}. \tag{4.11}$$

(ii) Order $n=3$: here we have 4 cases (see Fig. 8):

$$l_{ab}^{(3)}=R-2a+[O(a^3/R^2)],$$

$$\Lambda_{ab}^{(3)}=\frac{2R}{a}-[2+O(a/R)], \tag{4.12}$$

for $\mathbf{a}=1\cdot21\to\mathbf{b}=2\cdot12$ and permutations;

$$l_{ab}^{(3)}=R-\frac{2+3^{1/2}}{2}a+[O(a^2/R)],$$

$$\Lambda_{ab}^{(3)}=\frac{2R}{a}-[3^{1/2}+O(a/R)], \tag{4.13}$$

for $\mathbf{a}=1\cdot21\to\mathbf{b}=2\cdot13$ and permutations;

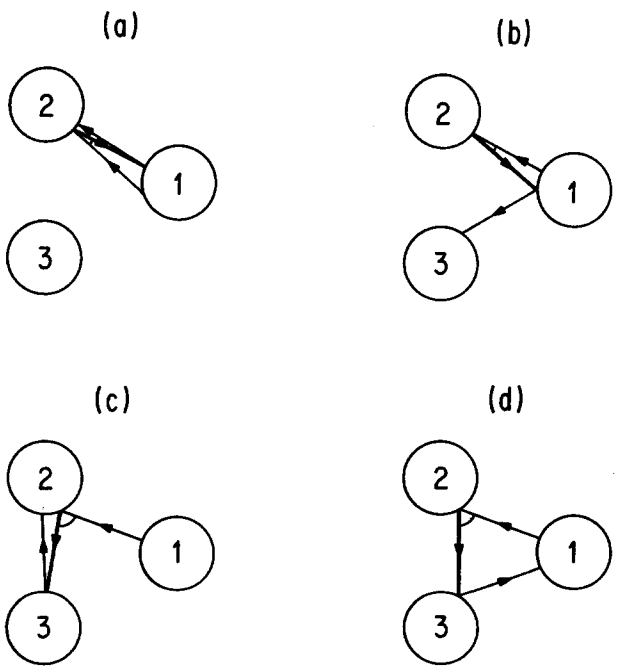

FIG. 8. Examples of the four different cases of flights at the $n=3$ approximation. The path length $l_{ab}^{(3)}$ is shown in heavy lines with the angle $\phi_a^{(3)}$. (a) flight $1\cdot21\to2\cdot12$; (b) flight $1\cdot21\to2\cdot13$; (c) flight $1\cdot23\to2\cdot32$; (d) flight $1\cdot23\to2\cdot31$.

$$l_{ab}^{(3)}=R-\frac{2+3^{1/2}}{2}a+[O(a^2/R)],$$

$$\Lambda_{ab}^{(3)}=\frac{4R}{3^{1/2}a}+[O(1)], \tag{4.14}$$

for $\mathbf{a}=1\cdot23\to\mathbf{b}=2\cdot32$ and permutations;

$$l_{ab}^{(3)}=R-3^{1/2}a+[O(a^2/R)],$$

$$\Lambda_{ab}^{(3)}=\frac{4R}{3^{1/2}a}+[O(1)], \tag{4.15}$$

for $\mathbf{a}=1\cdot23\to\mathbf{b}=2\cdot31$ and permutations. Here the $O(\cdots)$ means that this term cannot be determined without ambiguity because $\mathbf{a}$ denotes a domain but is not a point. When $n=3$, we observe that $l_{ab}^{(3)}$ is one order more precise than for $n=2$ but that $\Lambda_{ab}^{(3)}$ remains as badly defined as at order $n=2$ because of cases (c) and (d). Accordingly, the terms in brackets will be dropped at the $n=3$ approximation.

When $n=4$, $\Lambda_{ab}^{(4)}$ gains one order in precision. As $n\to\infty$, $\Lambda_{ab}^{(n)}$ and $l_{ab}^{(n)}$ converge to precise values. In this paper we shall use only the $n=2$ and $n=3$ approximations.

B. The Perron–Frobenius operator

We shall now construct the natural invariant measure μ as the limit of a sequence of invariant measures of Markov chains of increasing order. The limiting measure μ is, however, not Markovian.

The Markov chain constructed at order n of approximation is defined by the Perron–Frobenius operator, which defines the flow of probability in the dynamical system. Given our partition of the phase space, this operator may be represented by the matrix

$$Q_{ab}^{(n)}. \tag{4.16}$$

The labels $\mathbf{a}$ and $\mathbf{b}$ are n-tuples of symbols $\{1,2,3\}$; $\mathbf{a}$ corresponds to a cell as defined previously in Eqs. (4.5) and (4.6) and $\mathbf{b}$ is one of the possible images of cell $\mathbf{a}$ compatible with the transition matrix χ.

The flow between the discs stretches the cell $\mathbf{a}$ by the factor $\Lambda_{ab}^{(n)}$, hence cell $\mathbf{b}$ will retain a fraction $(\Lambda_{ab}^{(n)})^{-1}$ of the probability contained in cell $\mathbf{a}$; i.e., $Q_{ab}^{(n)}$ is proportional to $[\Lambda_{ab}^{(n)}]^{-1}$ (see Fig. 9). However, if we took $Q_{ab}^{(n)}=[\Lambda_{ab}^{(n)}]^{-1}$, the successive iterations Q^k of this matrix would vanish as k increases because $\Lambda_{ab}^{(n)}$ is greater than 1, and no invariant probability could then be defined. Nevertheless, we know that the repellor is not globally attracting, and loses particles with an escape rate γ. The natural invar-

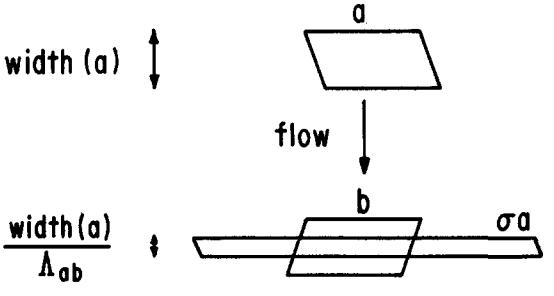

FIG. 9. Schematic geometry of the stretching mechanism.

iant measure is defined by the particles which remain on the repellor after a long time. As time increases, their number decreases, but the remaining ones have a past portion of their trajectory closer and closer to the repellor. If we assume the escape rate γ to be known, $Q_{\mathbf{ab}}^{(n)}$ must also be proportional to

$$e^{\gamma t_{\mathbf{ab}}^{(n)}}, \quad \gamma > 0, \tag{4.17}$$

where $t_{\mathbf{ab}}^{(n)}$ is the time between **a** and **b** and is given by

$$t_{\mathbf{ab}}^{(n)} = l_{\mathbf{ab}}^{(n)}/v, \tag{4.18}$$

where v is the velocity of the particle. This factor compensates the loss of probability due to particle escape with rate γ. Accordingly, we define the Perron–Frobenius operator by

$$Q_{\mathbf{ab}}^{(n)}(\gamma) = \frac{e^{\gamma t_{\mathbf{ab}}^{(n)}}}{\Lambda_{\mathbf{ab}}^{(n)}} \Xi_{\mathbf{ab}}^{(n)}. \tag{4.19}$$

$\Xi_{\mathbf{ab}}^{(n)}$ is the order n topological transition matrix defined as

$$\Xi_{\mathbf{ab}}^{(n)} = \chi_{a_1 b_1} \chi_{a_2 b_2} \cdots \chi_{a_n b_n}, \tag{4.20}$$

where χ is the order 1 topological transition matrix (3.10). For $n = 2$, $Q_{\mathbf{ab}}^{(2)}$ is a 6×6 matrix. For $n = 3$, $Q_{\mathbf{ab}}^{(3)}$ is a 12×12 matrix, etc.

C. The natural invariant measure

The value of the escape rate γ is, *a priori*, unknown. $Q_{\mathbf{ab}}^{(n)}$ will generate a normalizable probability measure if 1 is an eigenvalue of $Q_{\mathbf{ab}}^{(n)}$, i.e., if

$$\sum_{\mathbf{a}} u_{\mathbf{a}}^{(n)} Q_{\mathbf{ab}}^{(n)} = u_{\mathbf{b}}^{(n)}. \tag{4.21}$$

It is convenient to define the adjoint eigenvector $v_{\mathbf{a}}^{(n)}$:

$$\sum_{\mathbf{b}} Q_{\mathbf{ab}}^{(n)} v_{\mathbf{b}}^{(n)} = v_{\mathbf{a}}^{(n)}. \tag{4.22}$$

The escape rate $\gamma^{(n)}$ is determined as the smallest solution of

$$\det[I - Q^{(n)}(\gamma^{(n)})] = 0. \tag{4.23}$$

The other larger roots determine faster dynamics. Because $Q_{\mathbf{ab}}^{(n)}$ is a positive matrix and $\gamma^{(n)}$ is the smallest root, the eigenvectors $u_{\mathbf{a}}^{(n)}$ and $v_{\mathbf{b}}^{(n)}$ are positive.[30] Furthermore, we have

$$[(Q^{(n)})^k]_{\mathbf{ab}} \underset{k \to \infty}{\to} v_{\mathbf{a}}^{(n)} u_{\mathbf{b}}^{(n)}. \tag{4.24}$$

The invariant measure of probability is then defined as

$$\pi^{(n)}(\mathbf{a}) = u_{\mathbf{a}}^{(n)} v_{\mathbf{a}}^{(n)}, \tag{4.25}$$

if the eigenvectors $u_{\mathbf{a}}^{(n)}$ and $v_{\mathbf{a}}^{(n)}$ are normalized so that $\Sigma_{\mathbf{a}} \pi^{(n)}(\mathbf{a}) = 1$. We remark that $Q_{\mathbf{ab}}^{(n)}$ is *not* the matrix of transition probabilities of the Markov chain between **a** and **b**. This latter is given by

$$P_{\mathbf{ab}}^{(n)} = \frac{Q_{\mathbf{ab}}^{(n)} v_{\mathbf{b}}^{(n)}}{v_{\mathbf{a}}^{(n)}}. \tag{4.26}$$

The exact invariant measure π on the space S of the sequences **s** [see Eq. (3.13)] is obtained in the limit of large order n of the Markov chains,

$$\pi^{(n)} \underset{n \to \infty}{\to} \pi, \tag{4.27}$$

and we expect that the escape rate $\gamma^{(n)}$ determined at order n will similarly converge to the exact value γ:

$$\gamma^{(n)} \underset{n \to \infty}{\to} \gamma. \tag{4.28}$$

The natural invariant measure μ on the *flow* F [see Eq. (3.20)] is then defined as

$$\mu = \frac{\pi \otimes m}{(\pi \otimes m)(F)}, \tag{4.29}$$

where m is the Lebesque measure in the direction of the flow and $(\pi \otimes m)(F)$ is the normalizing factor. This measure acts on the Borel sets of the space F defining the repellor.

The Kolmogorov–Sinai entropy per unit time is the entropy of the Markov chain in the limit

$$h_{\mathrm{KS}} = \lim_{n \to \infty} -\frac{\Sigma_{\mathbf{a},\mathbf{b}} \pi^{(n)}(\mathbf{a}) P_{\mathbf{ab}}^{(n)} \log P_{\mathbf{ab}}^{(n)}}{\Sigma_{\mathbf{a}} t_{\mathbf{ab}}^{(n)} \pi^{(n)}(\mathbf{a})}, \tag{4.30}$$

where $t_{\mathbf{ab}}^{(n)}$ is the approximate time of flight between **a** and **b**, As n increases, $t_{\mathbf{ab}}^{(n)}$ converges to the time of flight $T(\mathbf{a})$ between **a** and $\sigma\mathbf{a}$ and $\Lambda_{\mathbf{ab}}^{(n)}$ converges to the value $\Lambda_{\mathbf{a}}$ (4.3) which is independent of **b**.

Given the preceding definitions, we prove the following:

$$h_{\mathrm{KS}} = \lambda_1 - \gamma \tag{4.31}$$

(see Appendix B).

D. The fast decay modes of the repellor

The smallest root of Eq. (4.23), γ_0, determines the slowest escape from the repellor, which corresponds to the asymptotic decay as time goes to infinity. However, for finite time the escape is dominated by the fast decay modes which are characterized by the other larger roots of Eq. (4.23), γ_k $(k = 1,2,\ldots)$, and their corresponding invariant measures μ_k.

In a scattering experiment, the incoming particles are described by a measure η (in general continuous with respect to the Lebesgue measure) which is decomposed on the complete set of invariant measures μ_k $(k = 0,1,2,\ldots)$.[25] The complete decay dynamics is thus

$$\eta = \sum_k c_k \mu_k e^{-\gamma_k t}, \tag{4.32}$$

with

$$\gamma_0 \leqslant \gamma_1 \leqslant \gamma_2 \leqslant \cdots, \tag{4.33}$$

and where the c_k are the expansion coefficients. In some problems, these fast decay modes may play a more important role than the asymptotic decay, which may become dominant only after the time interval of observation. Such a scenario may pertain in Hamiltonian systems[5] for which the decay dynamics is successfully modeled by a multiple exponential decay, albeit there is evidence that the asymptotic decay is governed by a power law.[16]

V. DETERMINATION OF THE HAUSDORFF DIMENSION

The repellor is a Cantor set characterized by a Hausdorff dimension $D_{\mathrm{H}} = d_{\mathrm{H}}^{(s)} + d_{\mathrm{H}}^{(u)} + 1$, where $d_{\mathrm{H}}^{(s)}$ $(d_{\mathrm{H}}^{(u)})$ is the Hausdorff dimension of the Cantor of the stable (unstable) manifold. The reversibility of the dynamics implies that

$d_{\mathrm{H}}^{(s)} = d_{\mathrm{H}}^{(u)} = d_{\mathrm{H}}$ and $D_{\mathrm{H}} = 2d_{\mathrm{H}} + 1$. We shall now determine the Hausdorff dimension by the following purely geometrical considerations based on the fractal properties of the repellor Ω_R.[31,33]

The unstable manifold of the Cantor set is a fractal of dimension d_{H}. We cover it with cells of width ϵ transverse to $W^{(u)}$ and of arbitrary length parallel to $W^{(u)}$. We assume that ϵ is much smaller than the cells **a** and **b**. We need

$$N(\epsilon) \sim \epsilon^{-d_{\mathrm{H}}} \tag{5.1}$$

such cells to cover the unstable manifold. These cells cover an area

$$\epsilon N(\epsilon) \sim \epsilon^{1-d_{\mathrm{H}}}. \tag{5.2}$$

A cell of width ϵ becomes a cell of width $\epsilon\Lambda_{\mathbf{ab}}^{(n)}$ after one iteration. The images of the cells now cover the area

$$(\epsilon\Lambda_{\mathbf{ab}}^{(n)})^{1-d_{\mathrm{H}}}, \tag{5.3}$$

so that the local self-similarity factor is

$$(\Lambda_{\mathbf{ab}}^{(n)})^{1-d_{\mathrm{H}}}. \tag{5.4}$$

Because the repellor Ω_R is invariant under the local stretching shown in Fig. 9, the factor (5.4) is compensated by the stretching factor $(\Lambda_{\mathbf{ab}}^{(n)})^{-1}$. We now define the Perron–Frobenius operator by

$$Q_{\mathbf{ab}}^{(n)}(d_{\mathrm{H}}) = \frac{1}{\Lambda_{\mathbf{ab}}^{(n)d_{\mathrm{H}}}} \Xi_{\mathbf{ab}}^{(n)}. \tag{5.5}$$

The order n topological transition matrix $\Xi^{(n)}$ is defined by Eq. (4.20). The dimension D_{H} is *a priori* unknown. Its value is determined, as previously, by requiring $Q^{(n)}$ to have the eigenvalue 1. The dimension $d_{\mathrm{H}}^{(n)}$ is the smallest solution of

$$\det[I - Q^{(n)}(d_{\mathrm{H}}^{(n)})] = 0. \tag{5.6}$$

For this value of d, $(Q^{(n)})^k$ is not vanishing and the invariant probability measure associated with $Q^{(n)}$ is defined as before [see Eqs. (4.21), (4.22), and (4.25)]. The exact value of d_{H} will be obtained in the limit of large n:

$$d_{\mathrm{H}}^{(n)} \underset{n\to\infty}{\to} d_{\mathrm{H}}. \tag{5.7}$$

VI. GENERALIZATION

We shall need, in the treatment of the quantum mechanical case, a generalization of the Perron–Frobenius operator. We observe that the two operators (4.19) and (5.5) are particular cases of the operator

$$Q_{\mathbf{ab}}^{(n)}(A,z) = \exp\left(\int_0^{t_{\mathbf{ab}}^{(n)}} \{A[X(t)] - z\}dt\right)\Xi_{\mathbf{ab}}^{(n)}, \tag{6.1}$$

where $A(X)$ is a function of the position X of the particle in the phase space. We recover Eq. (4.19) with

$$A(X) = -\kappa^{(u)}(X) \text{ and } z = -\gamma. \tag{6.2}$$

We recover Eq. (5.5) with

$$A(X) = -d_{\mathrm{H}}\kappa^{(u)}(X) \text{ and } z = 0. \tag{6.3}$$

The largest real value of z, which is a solution of

$$\det[I - Q^{(n)}(A,z)] = 0, \tag{6.4}$$

defines, in the limit $n\to\infty$, an invariant probability measure μ_A, associated with the quantity A and called the equilibrium measure. This solution, $z = P^{(n)}(A)$, is called the topological pressure. Its exact value is obtained by the limit,

$$P^{(n)}(A) \underset{n\to\infty}{\to} P(A) \tag{6.5}$$

which equals, in general,[32]

$$z = P(A) = h_{\mathrm{KS}}(\mu_A) + \int A(X)\mu_A(dX). \tag{6.6}$$

Furthermore, we have the inequality

$$P(A) > h_{\mathrm{KS}}(\mu) + \int A(X)\mu(dX), \tag{6.7}$$

when μ is an invariant measure different from the equilibrium measure μ_A. This property is called the variational principle of Ruelle, Bowen, and Sinai.[32]

When $A = -\kappa^{(u)}$, Eq. (4.31) is recovered from the general result (6.6) with $\gamma = -P(A)$. When $A = -d\kappa^{(u)}$, the pressure $P(A)$ is a function of the parameter d. The Lyapunov exponent λ_1 is then given by minus the derivative of this function with respect to the parameter d at the value $d = 1$:

$$\lambda_1 = -[P(-d\kappa^{(u)})]'_{d=1}. \tag{6.8}$$

This result follows from Eq. (6.6) and from the variational principle. The information dimension d_I can then be calculated using Eq. (2.9). On the other hand, the Hausdorff dimension d_{H} is the value of the parameter d which is solution of the equation:

$$P(-d_{\mathrm{H}}\kappa^{(u)}) = 0. \tag{6.9}$$

VII. THE ZETA FUNCTION OF RUELLE

In the quantum mechanical treatment discussed elsewhere,[36] we shall need to use the Ruelle zeta function defined for a flow as[34]

$$\zeta_A(z) = \prod_{\omega}\left\{1 - \exp\int_0^{T_\omega}[A(\Phi^t X_\omega) - z]dt\right\}^{-1}, \tag{7.1}$$

where the product extends over the periodic orbits ω of the flow, and T_ω is the fundamental period of ω. X_ω is an arbitrary point on ω. For a flow constructed as in Sec. III, and with the definition

$$\alpha(\mathbf{s}) = \int_0^{T(\mathbf{s})} A[\Phi^t J(\mathbf{s})]dt, \tag{7.2}$$

we have

$$\zeta_A(z) = \exp\sum_{n=1}^{\infty}\frac{1}{n}\sum_{\omega}\exp\left[\int_0^{nT_\omega} A(\Phi^t X_\omega)dt - znT_\omega\right]$$
$$= \exp\sum_{m=1}^{\infty}\frac{1}{m}\sum_{\mathbf{s}\in fix\sigma^m}\exp\sum_{k=0}^{m-1}[\alpha(\sigma^k\mathbf{s}) - zT(\sigma^k\mathbf{s})], \tag{7.3}$$

where we have used

$$\frac{1}{1-y} = \exp\sum_{n=1}^{\infty}\frac{y^n}{n}. \tag{7.4}$$

Using the definition (6.1), we can rewrite Eq. (7.3) as follows:

$$\zeta_A^{(n)}(z) = \exp \sum_{m=1}^{\infty} \frac{1}{m} \sum_{s \in fix\, \sigma^m} Q^{(n)}_{s,\sigma s} Q^{(n)}_{\sigma s,\sigma^2 s} \cdots Q^{(n)}_{\sigma^{m-1} s,s}, \quad (7.5)$$

where $Q^{(n)}_{s,\sigma s}$ is the matrix element $Q^{(n)}_{ab}$ for which $s \in a$ and $\sigma s \in b$. We remark that Eq. (7.5) is valid because the cells **a** have no boundary in common. If some periodic trajectories existed on the common boundaries of several cells **a**, the result would be more complicated than Eq. (7.5).[35] From Eq. (7.5),

$$\zeta_A^{(n)}(z) = \exp \sum_{m=1}^{\infty} \frac{1}{m} \operatorname{Tr} Q^{(n)m} \quad (7.6)$$

and

$$\zeta_A^{(n)}(z) = \frac{1}{\det[I - Q^{(n)}(A,z)]}. \quad (7.7)$$

This expansion is valid for all the Markov chains of order n. In the limit $n \to \infty$, the zeta function $\zeta_A(z)$ is obtained:

$$\zeta_A^{(n)}(z) \underset{n\to\infty}{\to} \zeta_A(z). \quad (7.8)$$

The function ζ_A is known to be analytic in the half-plane

$$\operatorname{Re} z > P(A), \quad (7.9)$$

with a simple pole at $P(A)$, but it may have poles in the half-plane

$$\operatorname{Re} z \leqslant P(A). \quad (7.10)$$

In this half-plane ζ_A is a meromorphic function.[32,34]

VIII. RELATIONSHIPS BETWEEN THE 3 HARD DISC AND THE 2 HARD DISC SYSTEMS

Consider the geometry shown in Fig. 10. Now the radius a' of disc 3 may be different from the radius a of discs 1 and 2. The classical properties of this repellor in the limit of large R and R' are well approximated by the Perron–Frobenius operator at order $n = 2$. Then $Q^{(2)}_{ab}(\gamma,d)$ is given by the 6×6 matrix

$$\begin{array}{c} \\ 1\cdot2 \\ 1\cdot3 \\ 2\cdot1 \\ 2\cdot3 \\ 3\cdot1 \\ 3\cdot2 \end{array} \begin{array}{c} \begin{array}{cccccc} 1\cdot2 & 1\cdot3 & 2\cdot1 & 2\cdot3 & 3\cdot1 & 3\cdot2 \end{array} \\ \begin{bmatrix} 0 & 0 & x & z & 0 & 0 \\ 0 & 0 & 0 & 0 & y & t \\ x & z & 0 & 0 & 0 & 0 \\ 0 & 0 & 0 & 0 & t & y \\ w & y & 0 & 0 & 0 & 0 \\ 0 & 0 & w & y & 0 & 0 \end{bmatrix} \end{array} \quad (8.1)$$

with

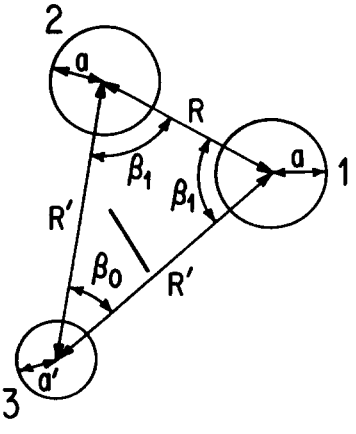

FIG. 10. The geometry of the 3HD system when disc 3 is far from discs 1 and 2.

$$x = \left(\frac{a}{2R}\right)^d e^{\gamma R/v}, \quad z = \left[\frac{a\cos(\beta_1/2)}{2R'}\right]^d e^{\gamma R'/v},$$
$$y = \left(\frac{a'}{2R'}\right)^d e^{\gamma R'/v}, \quad t = \left[\frac{a'\cos(\beta_0/2)}{2R'}\right]^d e^{\gamma R'/v},$$
$$w = \left[\frac{a\cos(\beta_1/2)}{2R}\right]^d e^{\gamma R/v}. \quad (8.2)$$

We have

$$0 = \det(Q^{(2)} - I)$$
$$= [1 - x + (t+y)(xy - wz - y)]$$
$$\times [1 + x + (t-y)(xy - wz + y)]. \quad (8.3)$$

Only the first polynomial is relevant here because it possesses a real root although the corresponding root of the second polynomial is complex.

A. Limit $a' \ll a$

Noting that y and t are vanishing when $a' \to 0$, we obtain for $d = 1$ the escape rate

$$\gamma = \frac{v}{R} \ln \frac{2R}{a} + O(a'), \quad (8.4)$$

and, for $\gamma = 0$,

$$d_H \simeq \frac{1}{\ln \dfrac{R'}{a'}}. \quad (8.5)$$

We observe that d_H goes to zero as $a' \to 0$, as expected. The Lyapunov exponent is calculated using Eq. (6.8). The result is

$$\lambda_1 \simeq \frac{v}{R}\left[\ln \frac{2R}{a} + O\left(\frac{a'}{R'} \ln \frac{R'}{a'}\right)\right]. \quad (8.6)$$

As $a' \to 0$, $\gamma = \lambda_1$ and the entropy given by Eq. (4.31) vanishes, as expected, because the repellor contains only a single unstable periodic orbit when the point particle is scattered from two discs.

B. Limit $a' = a$, $R' \gg R$

As observed in Eqs. (8.2), x and w are proportional to $e^{\gamma R/v}$, but y, z, and t to $e^{\gamma R'/v}$. As a consequence, the first polynomial in Eq. (8.3) reduces to

$$xy - wz = y, \quad (8.7)$$

in the limit $R' \gg R$. Equation (8.7) is equivalent for $d = 1$ to

$$\frac{a}{2R}[\sin(\beta_1/2)]^2 e^{\gamma R/v} = 1. \quad (8.8)$$

Because $\beta_1 \simeq \pi/2 - R/2R'$ for large R', we obtain the result,

$$\gamma \simeq \frac{v}{R} \ln \frac{4R}{a}. \quad (8.9)$$

We note that Eq. (8.9) is different from the escape rate of the two disc repellor. Indeed, the escape rate is proportional to the inverse of the time of flight between the discs but only to the logarithm of the distance between the discs. Consequently, when $R' \gg R$ the escape between disc 3 and the two other discs is negligible with respect to the escape between discs 1

and 2. However, in addition to the flights 121 and 212, the flights 321 and 312 also contribute to the escape rate between discs 1 and 2, and by amounts of the same order. It follows that the escape rate of the complete three disc repellor is larger than the escape rate of the two disc repellor obtained previously in Eq. (8.4).

IX. THREE HARD DISC SYSTEM AT ORDER $n=2$

As shown in Sec. IV, at order $n=2$ the distance between the discs is not approximated better than R [see Eq. (4.10)]. The local Lyapunov numbers are given by Eq. (4.11). By setting

$$x=\left(\frac{a}{2R}\right)^d e^{\gamma R/v}, \tag{9.1}$$

$$w=\left(\frac{3^{1/2}a}{4R}\right)^d e^{\gamma R/v}, \tag{9.2}$$

the Perron–Frobenius operator $Q^{(2)}_{ab}(\gamma,d)$ becomes

$$\begin{array}{c} \\ 1\cdot2 \\ 1\cdot3 \\ 2\cdot1 \\ 2\cdot3 \\ 3\cdot1 \\ 3\cdot2 \end{array}\begin{array}{c} \begin{array}{cccccc} 1\cdot2 & 1\cdot3 & 2\cdot1 & 2\cdot3 & 3\cdot1 & 3\cdot2 \end{array} \\ \begin{bmatrix} 0 & 0 & x & w & 0 & 0 \\ 0 & 0 & 0 & 0 & x & w \\ x & w & 0 & 0 & 0 & 0 \\ 0 & 0 & 0 & 0 & w & x \\ w & x & 0 & 0 & 0 & 0 \\ 0 & 0 & w & x & 0 & 0 \end{bmatrix} \end{array} \tag{9.3}$$

and we obtain

$$\det[I-Q^{(2)}] = (1-w-x)(1-w+x)(1+w+w^2-x^2)^2. \tag{9.4}$$

If we introduce the definition

$$\xi=\left(\frac{a}{R}\right)^d e^{\gamma R/v}, \tag{9.5}$$

Eqs. (9.1) and (9.2) become

$$x=(1/2)^d\xi \quad \text{and} \quad w=(3^{1/2}/4)^d\xi, \tag{9.6}$$

and the roots of the polynomial in ξ are

$$\xi_1=\frac{1}{(3^{1/2}/4)^d+(1/2)^d}, \tag{9.7}$$

$$\xi_2,\xi_3=\frac{3^{d/2}\mp(4^{d+1}-3^{d+1})^{1/2}}{2[1-(3/4)^d]}, \tag{9.8}$$

$$\xi_4=\frac{1}{(3^{1/2}/4)^d-(1/2)^d}. \tag{9.9}$$

These roots are ordered as follows:

$$|\xi_1|<|\xi_2|<|\xi_3|<|\xi_4|. \tag{9.10}$$

If we set $d=1$,

$$\xi_1=\frac{4}{2+3^{1/2}}, \tag{9.11}$$

and Eq. (9.4) reduces to Eq. (4.23), with the escape rate determined by its smallest root:

$$\gamma^{(2)}=\frac{v}{R}\ln\frac{4R}{(2+3^{1/2})a}. \tag{9.12}$$

On the other hand, by setting $\gamma=0$ in Eq. (9.4) we obtain Eq. (5.6), with the Hausdorff dimension determined by its smallest root:

$$d_H^{(2)}\simeq\frac{\ln 2}{\ln R/a}. \tag{9.13}$$

From Eqs. (6.8) and (4.31), the Lyapunov exponent and the entropy are

$$\lambda_1^{(2)}=\frac{v}{R}\left(\ln\frac{R}{a}+\frac{3^{1/2}}{2+3^{1/2}}\ln\frac{4}{3^{1/2}}+\frac{2}{2+3^{1/2}}\ln 2\right) \simeq\frac{v}{R}\ln\frac{2.138\,07R}{a}, \tag{9.14}$$

$$h_{KS}^{(2)}\simeq\frac{v}{R}\ln 1.994\,85. \tag{9.15}$$

The information dimension as given by Eq. (2.9) is

$$d_I^{(2)}\simeq\frac{\ln 1.994\,85}{\ln R/a}, \tag{9.16}$$

so that the difference with respect to the Hausdorff dimension (9.13) is small for large R. The entropy per unit time is positive for any fixed R and takes a value near ln 2 in units of the time of flight R/v. This value has its origin in the fact that the topological Markov chain has an entropy

$$h_{top}=\ln 2 \tag{9.17}$$

[see Eq. (3.11)], meaning that the symbols in a sequence **s** are chosen from two possibilities according to the transition matrix χ: if we have symbol 1, the next will be 2 or 3. Since $h_{KS}>0$, the Lyapunov exponent λ_1 is different from the escape rate γ. The values given above for λ_1, h_{KS} and d are valid for $R\to\infty$. We expect them to hold at any order $n=3,4,\ldots$. We shall check this claim for $n=3$ in the next section.

X. THREE HARD DISC SYSTEM AT ORDER $n=3$

As shown in Sec. IV, at order $n=3$ the precision of calculation of Lyapunov numbers is not increased but the distances between the discs are more precisely defined. [See Eqs. (4.12)–(4.15).] Here we shall define the matrix elements by

$$x=\left(\frac{a}{2R}\right)^d e^{(\gamma/v)(R-2a)}, \tag{10.1}$$

$$z=\left(\frac{3^{1/2}a}{4R}\right)^d e^{(\gamma/v)[R-(1+3^{1/2}/2)a]}, \tag{10.2}$$

$$y=\left(\frac{a}{2R}\right)^d e^{(\gamma/v)[R-(1+3^{1/2}/2a]}, \tag{10.3}$$

$$w=\left(\frac{3^{1/2}a}{4R}\right)^d e^{(\gamma/v)(R-3^{1/2}a)}. \tag{10.4}$$

We observe that

$$xw=yz, \tag{10.5}$$

which will simplify expressions later. Now the Perron–Frobenius operator $Q^{(3)}_{ab}$ is a 12×12 matrix given by the following array (where the blanks are zeros):

$$
\begin{array}{c|cccccccccccc}
 & 1\cdot21 & 1\cdot31 & 2\cdot12 & 2\cdot32 & 3\cdot13 & 3\cdot23 & 1\cdot23 & 1\cdot32 & 2\cdot13 & 2\cdot31 & 3\cdot12 & 3\cdot21 \\
1\cdot21 & & & x & & & & & & y & & & \\
1\cdot31 & & & & & x & & & & & & y & \\
2\cdot12 & x & & & & & & y & & & & & \\
2\cdot32 & & & & & & x & & & & & & y \\
3\cdot13 & & x & & & & & & y & & & & \\
3\cdot23 & & & & x & & & & & & y & & \\
1\cdot23 & & & & z & & & & & & w & & \\
1\cdot32 & & & & & & z & & & & & & w \\
2\cdot13 & & z & & & & & & w & & & & \\
2\cdot31 & & & & & z & & & & & & w & \\
3\cdot12 & z & & & & & & w & & & & & \\
3\cdot21 & & & z & & & & & & w & & &
\end{array}
\tag{10.6}
$$

The characteristic equation is

$$\det[I - Q^{(3)}] = (1 - w - x + xw - yz)(1 - w + x - xw + yz)[1 + w + w^2 - x^2 - x(xw - yz) - (xw - yz)^2]^2. \tag{10.7}$$

Noting Eq. (10.5) we find

$$\det[I - Q^{(3)}] = (1 - w - x)(1 - w + x)(1 + w + w^2 - x^2)^2, \tag{10.8}$$

which is the same polynomial as Eq. (9.4) at order $n = 2$. Note, however, that the exponential factors in x and w are different, and we cannot solve the preceding equation as in Sec. IX. We proceed as follows. For R large enough, the values for γ and d obtained from Eq. (10.8) will reduce to the ones obtained at order $n = 2$. We can thus make an expansion in a/R to obtain

$$\gamma^{(3)} = \frac{v}{R}\left[\ln\frac{4R}{(2+3^{1/2})a}\right]\left[1 + \frac{7a}{(2+3^{1/2})R}\right], \tag{10.9}$$

$$d_{\mathrm{H}}^{(3)} \simeq \frac{\ln 2}{\ln R/a}, \tag{10.10}$$

which is an improvement relative to $\gamma^{(2)}$.

We can also numerically solve Eq. (10.8) by the Newton–Raphson method. We note that the polynomial of interest is

$$1 - w - x, \tag{10.11}$$

which gives the smallest root of Eq. (10.8). We solve by the Newton–Raphson method the equation

$$f(t) = 1 + \left(\frac{2}{3^{1/2}}\right)^d e^{-(2-3^{1/2})at} - \left(\frac{4R}{3^{1/2}a}\right)^d e^{-(R-3^{1/2}a)t}, \quad a = 1, \tag{10.12}$$

$$t_{k+1} = t_k - \frac{f(t_k)}{f'(t_k)}, \quad t_0 = 0. \tag{10.13}$$

Here $d = 1$, and we put $t = \gamma^{(3)}/v$. After 20 iterations the results shown in Table I are obtained. We observe that both orders ($n = 2$, $n = 3$) become consistent to one significant figure for $R > 10$, which we take as the limit of validity of order $n = 2$. The results for $n = 3$ remain valid for smaller R.

The similarity between the determinants at order $n = 2$ and $n = 3$ is interesting and has its origin in the following consideration. As shown before, the repellor is enclosed in 12 cells. These cells are subdivided into two classes. As shown in Fig. 6, there are 6 cells centered around $\phi = \pi$ and 6 other cells. We can simplify the Markov chain by defining two new domains

$$A = 1\cdot21 \cup 1\cdot31 \cup 2\cdot12 \cup 2\cdot32 \cup 3\cdot13 \cup 3\cdot23, \tag{10.14}$$

$$B = 1\cdot23 \cup 1\cdot32 \cup 2\cdot13 \cup 2\cdot31 \cup 3\cdot12 \cup 3\cdot21. \tag{10.15}$$

The Perron–Frobenius operator Q of the new Markov chain is

TABLE I. Escape rates for velocity $v = 1$ at the $n = 2$ and $n = 3$ approximations compared with the numerical simulation results, for various interdisc distances R.

R	Order $n = 2$	Order $n = 3$	Numerical
2.05	···	···	0.252
2.1	···	···	0.440
2.3	···	···	0.694
2.5	···	···	0.715
2.7	···	···	0.713
3.0	···	···	0.665
3.5	0.3777	0.8103	0.602
4.0	0.3639	0.6832	0.567
4.5	0.3496	0.5983	0.509
5.0	0.3358	0.5365	0.461
5.5	0.3226	0.4889	0.439
6.0	0.3102	0.4508	0.410
7.0	0.2879	0.3930	0.354
8.0	0.2686	0.3507	0.314
9.0	0.2518	0.3180	0.284
10.0	0.2372	0.2919	0.278
12.5	0.2076	0.2442	0.221
15.0	0.1852	0.2116	0.205
17.5	0.1675	0.1876	0.172
20.0	0.1533	0.1691	0.158
40.0	0.0940	0.0986	···
80.0	0.0556	0.0570	···

$$\begin{array}{c} \\ A \\ B \end{array} \begin{array}{c} \begin{array}{cc} A & B \end{array} \\ \begin{bmatrix} x & y \\ z & w \end{bmatrix} \end{array} \tag{10.16}$$

with the characteristic equation

$$\det(I-Q) = 1 - w - x + xw - yz \tag{10.17}$$

from which the first polynomial of determinant Eq. (10.7) is recovered. Thus the simplified Markov chain contains all the relevant information (i.e., escape rate and Hausforff dimension) of the classical dynamics. However, the semiclassical quantum dynamics is determined by the full matrix.

XI. THREE HARD DISCS CLOSE TOGETHER AND THE *N* HARD DISC SYSTEM

A. Bottleneck effect for small interdisc spacing

Thus far we have considered the dynamical properties of the 3HD system (i.e., escape rate and dimension), in the limit of large spacing between the discs. In this limit the repellor becomes filamentary, the dimension of the repellor tends to one and the rate of escape of the point particle from the repellor is described by the asymptotic formulas Eq. (9.12) or Eq. (10.9).

The calcuation of the dynamical properties in the limit where the three discs are close together is also tractable. When $R \approx 2a$, the escape rate is low and the point particle is in quasiequilibrium inside the trap formed by the discs. The escape rate can be calculated to be

$$\gamma = v \frac{12(R-2a)}{\pi(3^{1/2}R^2 - 2\pi a^2)}, \tag{11.1}$$

and the repellor is bulky with a dimension nearly equal to

$$D_I = 2d_I + 1 \approx 3. \tag{11.2}$$

As a consequence, the Lyapunov exponent is approximately equal to the entropy per unit time and both are greater than the escape rate [see Eqs. (2.12) and (2.13)]. When $R = 2a$ the escape rate vanishes since the interior region is then closed. When $R \approx 2a$ the Eyring theory can be applied to the point particle-3HD system because the lifetime $1/\gamma$ of the metastable state is longer than the randomization time $1/h_{KS}$.

B. Large cluster of hard discs

When there are a large number of hard discs close together, for instance forming a wide shell which is periodic in the y direction (see Fig. 11), a point particle in the interior of the shell can be described using the quasiequilibrium approximation. From the work of Machta and Zwanzig,[27] and of Bunimovich and Sinai,[13] we know that a point particle trapped in this Lorentz lattice undergoes Brownian motion with a diffusion coefficient

$$\mathscr{D} = v \frac{R^2(R-2a)}{\pi(3^{1/2}R^2 - 2\pi a^2)}. \tag{11.3}$$

This result is valid when the system has a finite horizon, i.e., when a point particle can not pass through the shell of discs, in any direction, without collision. This condition is met, in a triangular lattice, when

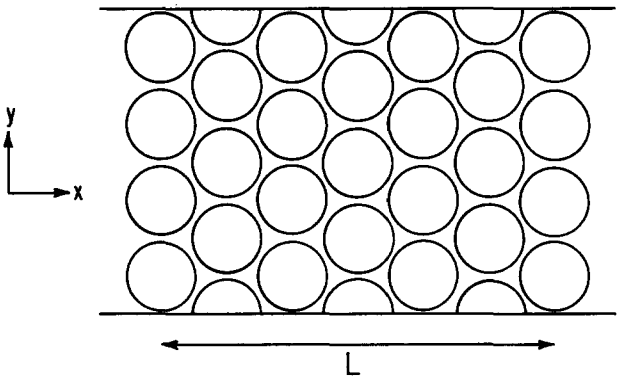

FIG. 11. A wide shell of hard discs with periodic conditions in the y direction. The width is L.

$$R < \frac{4a}{3^{1/2}}. \tag{11.4}$$

Accordingly, when the width of the shell of discs is large, we can approximate the motion of the point particle using a diffusion equation:

$$\partial_t f = \mathscr{D}\partial_x^2 f. \tag{11.5}$$

Suppose the shell of discs extends from $-L/2$ to $L/2$. Let f be the distribution function for point particles, i.e., the density as a function of space and time in an ensemble generated by N_0 experiments in which a point particle is incident on the shell of discs. We are interested in f in the interior of the shell and we require that $f = 0$ outside the shell. The relevant solution of Eq. (11.5) is

$$f(x,t) = \sum_{n=0}^{\infty} c_n e^{-\gamma_n t} \sin k_n (L/2 - x), \tag{11.6}$$

with

$$k_n = \frac{\pi}{L}(n+1), \quad \gamma_n = \mathscr{D}k_n^2. \tag{11.7}$$

Equation (11.5) is only valid when $2\pi/k_n \gg R$; it describes the long time behavior of the population dynamics. For $t \to \infty$ we have

$$f(x,t) \simeq c_0 e^{-\gamma_0 t} \sin(\pi/2 - \pi x/L). \tag{11.8}$$

The number of point particles still trapped at time t is

$$N(t) = \int_{-L/2}^{L/2} f(x,t)dx \simeq \frac{2Lc_0}{\pi} e^{-\gamma_0 t}, \tag{11.9}$$

so that the escape rate is

$$\gamma = \mathscr{D}\left(\frac{\pi}{L}\right)^2, \tag{11.10}$$

where the diffusion coefficient $\mathscr{D}$ is given by Eq. (11.3). Finally,

$$\gamma = v \frac{R^2}{L^2} \frac{\pi(R-2a)}{(3^{1/2}R^2 - 2\pi a^2)}. \tag{11.11}$$

Although the hard disc–point particle scatterer system is deterministic with only two degrees of freedom, its dynamics can be modeled by the diffusion equation (11.5) because the system has a finite horizon, large spatial extension and defocusing dynamics, which nicely illustrates the interplay between reversible microscopic dynamics and irreversible macroscopic dynamics.

XII. NUMERICAL SIMULATIONS AND DISCUSSION

The escape rate in the point particle–three hard disc system is understood in two domains: (i) When the discs are close together the escape rate is given by Eq. (11.1), which shows how $\gamma \to 0$ as $R \to 2a$, exhibiting a bottleneck effect. (ii) When the discs are far apart, the escape rate is given by Eqs. (9.12) and (10.9), which shows how $\gamma \to 0$ as $R \to \infty$, exhibiting a damping of the escape rate due to the long time of flight between the discs. Note that in this latter case the time of flight is proportional to $1/R$ and the defocusing contributes only a factor $\ln R$ to the escape rate. Between these two extreme cases, we expect a maximum for the point particle escape rate.

We have carried out a numerical simulation of the point particle–three hard disc system. The trajectory of the point particle was calculated for a large number N_0 of initial conditions, and from the trajectories we calculated the number N_t of particles present in a large ball of radius b at time t. The escape rate γ is obtained from the slope of a straight line fitted through the curve $\ln N_t$ vs t. The escape rates were calculated for different values of the interdisc distance R. The results are displayed in Fig. 12 and reported in Table I, along with the predictions of Eqs. (9.12) and (10.9) (the $n = 2$ and $n = 3$ approximations, respectively). We observe that the agreement is excellent. Note that exact values of γ as a function of R are bounded between the two approximations Eqs. (9.12) and (10.9), suggesting an oscillatory convergence for the sequence (4.28) as the order of approximation increases.

XIII. CONCLUSIONS

We have analyzed the rate of escape of a point particle from a filamentary chaotic repellor. The dynamics of motion are very different in this case from those characteristic of a bulky repellor, for which the quasiequilibrium hypothesis is applicable. We find that the fractal geometry of the repellor plays an important role when it is filamentary. The point particle–three hard disc system considered here has chaotic dynamics; we are able to construct its repellor using a coding of the dynamics and of the fractal geometry exploiting the partition shown in Fig. 6.

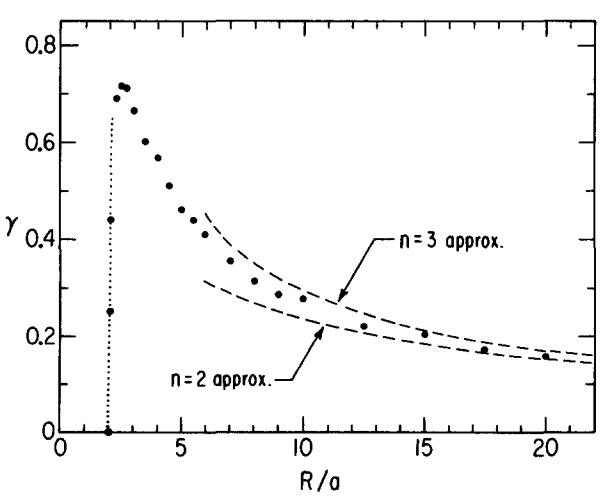

FIG. 12. The escape rate γ for velocity $v = 1$ vs the interdisc distance R. The dots are the results of our numerical simulation. The dashed lines are the $n = 2$ and $n = 3$ approximations given in Table I for large R. The dotted line is the slope at $R = 2a$ of the quasiequilibrium approximation given by Eq. (11.1). The number of initial conditions N_0 is 10^5 for small R and 10^6 for large R.

As discussed in Sec. I, the point particle–three hard disc system dynamics is simplified by the absence of quasiperiodic islands in the repellor. The present work is thus of direct application in any scattering system for which we may assume that *no stable periodic orbit exists in the classical dynamics, or if such stable periodic orbits make negligible contributions to the system dynamics.* Other examples of such systems are a particle incident on three or more fixed scattering centers with a general repulsive potential, the incident particle having an energy large relative to the depths of the potential wells.

The most important result of the research reported in this paper is the method developed to calculate the escape rate, namely requiring the eigenvalue 1 for the Perron–Frobenius operator (see Secs. IV and VIII to X). This calculation is nontrivial because the repellor is chaotic. We find that the escape of the point particle from the repellor is inhibited by the randomization of the trajectories, as expressed in Eq. (2.12) or Eq. (4.31). This result is fundamental to our analysis because it connects a physical property, namely the particle escape rate, to a defined property, namely the entropy per unit time. The escape rate and the entropy per unit time define two time scales characterizing the repellor: its lifetime and its randomization time. When the repellor is bulky the lifetime is longer than the randomization time. However, the lifetime is shorter than the randomization time when the repellor is filamentary.

The simplicity of the point particle–hard disc model allows us to clarify the relationship between the transport properties of a point particle in a hard disc lattice, such as the diffusion coefficient, and the escape rate of a point particle from a large cluster of hard discs. In such large systems the randomization time remains microscopic albeit the lifetime becomes macroscopic. The diffusion time, $t_{\text{diff}} = R^2/\mathscr{D}$, also remains microscopic but is longer than the randomization time: $1/h_{\text{KS}} < t_{\text{diff}} \ll 1/\gamma$. The Kolmogorov–Sinai entropy per unit time defines the randomization time scale. At this characteristic time, a crossover occurs between deterministic system dynamics based on individual trajectories and statistical system dynamics based on probabilistic ensembles of trajectories.

In the course of our analysis we have introduced the Ruelle zeta function and showed how to calculate it in terms of the Perron–Frobenius operator. [See Eqs. (7.7), (9.4), and (10.8).] The importance of this zeta function will become evident in the following paper, where we shall report the results of semiclassical quantization of the point particle–three hard disc system.

ACKNOWLEDGMENTS

The authors are grateful to G. Paladin for fruitful discussions. P. G. is "Chargé de Recherches" at the National Fund for Scientific Research (Belgium). This research was supported by a grant from the National Science Foundation.

APPENDIX A

In a dynamical system with quasiperiodic islands, the rate of escape from the repellor is expected to follow a power-law decay (2.11) because of successive trappings of a trajectory inside the hierarchy of quasiperiodic islands.[16,17] This power law behavior refers to the properties of an ensemble of scattering experiments in which there is a single incident energy E.

However, there is a *different* effect which can also produce a power-law decay *even* in the case of completely chaotic dynamics, i.e., *without* quasiperiodic islands. Such a power law occurs if the ensemble of incident particles has an energy distribution extending to zero energy. If $\rho(v)$ is the density of the distribution of incident velocities,

$$\frac{N_t}{N_0} = \int_0^\infty d^f v \rho(v) C(mv^2/2) e^{-v\bar{\gamma}t}. \tag{A1}$$

If $\rho(0)$ is a nonvanishing constant

$$\frac{N_t}{N_0} \sim \frac{1}{t^f}. \tag{A2}$$

In our example $f = 2$. The escape from B is very slow because it is dominated by very slow free particle motion. To avoid complications associated with the long time tail of N_t/N_0 for scattering events with near zero incident energy, we assume we need deal with only those scattering events with nonzero incident energy. We note that the same effect is also present in the quantum dynamics[28] where it guarantees compatibility with the Paley–Wiener theorem.[29]

APPENDIX B

We prove here Eq. (4.31) with the assumptions of Sec. IV. We shall drop the label (n) and suppose that the order n is large enough. Using Eqs. (4.15) and (4.26), the entropy (4.30) becomes

$$h_{\rm KS} \approx -\frac{1}{\sum_{\mathbf{a}} T(\mathbf{a})\pi(\mathbf{a})} \sum_{\mathbf{ab}} u_{\mathbf{a}} v_{\mathbf{a}} \frac{Q_{\mathbf{ab}} v_{\mathbf{b}}}{v_{\mathbf{a}}} \log \frac{Q_{\mathbf{ab}} v_{\mathbf{b}}}{v_{\mathbf{a}}}. \tag{B1}$$

Using the definition of the Perron–Frobenius operator (4.19),

$$h_{\rm KS} \approx -\frac{1}{\sum_{\mathbf{a}} T(\mathbf{a})\pi(\mathbf{a})} \sum_{\mathbf{ab}} u_{\mathbf{a}} Q_{\mathbf{ab}} v_{\mathbf{b}} [\gamma T(\mathbf{a}) - \log \Lambda_{\mathbf{a}} + \log v_{\mathbf{b}} - \log v_{\mathbf{a}}]. \tag{B2}$$

Then using Eqs. (4.21), (4.22), and (4.25),

$$h_{\rm KS} \approx -\gamma + \frac{1}{\sum_{\mathbf{a}} T(\mathbf{a})\pi(\mathbf{a})} \sum_{\mathbf{a}} \pi(\mathbf{a}) \log \Lambda_{\mathbf{a}}. \tag{B3}$$

Finally, using the definition of $\Lambda_{\mathbf{a}}$ (4.3),

$$h_{\rm KS} \approx -\gamma + \frac{1}{\sum_{\mathbf{a}} T(\mathbf{a})\pi(\mathbf{a})} \sum_{\mathbf{a}} \pi(\mathbf{a}) \int_{t_{\mathbf{a}}}^{t_{\mathbf{a}}} \kappa^{(u)}[X(t)]dt. \tag{B4}$$

The second term of Eq. (B4) is the average value of the local Lyapunov exponent. By the definition Eq. (4.29) of the invariant measure μ, and by its ergodicity,

$$h_{\rm KS} \approx -\gamma + \sum_{\mathbf{a}} \int_{\mathbf{a}} \kappa^{(u)}(X)\mu(dX), \tag{B5}$$

which leads to Eq. (4.31) after use of the definition (4.2) of the Lyapunov exponent λ_1.

[1] D. Bensimon and L. P. Kadanoff, Physica D **13**, 82 (1984).
[2] R. S. MacKay, J. D. Meiss, and I. C. Percival, Physica D **13**, 55 (1984).
[3] M. J. Davis, J. Chem. Phys. **83**, 1016 (1985).
[4] M. J. Davis and S. K. Gray, J. Chem. Phys. **84**, 5389 (1986).
[5] S. K. Gray, S. A. Rice, and M. J. Davis, J. Phys. Chem. **90**, 3470 (1986).
[6] S. K. Gray and S. A. Rice, J. Chem. Phys. **86**, 2020 (1987).
[7] B. Eckhardt, J. Phys. A **20**, 5971 (1987).
[8] D. W. Noid, S. K. Gray, and S. A. Rice, J. Chem. Phys. **84**, 2649 (1986); B. Eckhardt and C. Jung, J. Phys. A **19**, L829 (1986); C. Jung and H. J. Scholz, *ibid.* **20**, 3607 (1987).
[9] A. J. Lichtenberg and M. A. Lieberman, *Regular and Stochastic Motion* (Springer, New York, 1983); V. I. Arnold and A. Avez, *Ergodic Problems of Classical Mechanics* (Benjamin, New York, 1968).
[10] M. Henon and C. Heiles, Astron. J. **69**, 73 (1964); G. H. Walker and J. Ford, Phys. Rev. **188**, 416 (1969).
[11] N. Wiener, *The Fourier Integral and Certain of its Applications* (Dover, New York, 1958).
[12] R. Kosloff and S. A. Rice, J. Chem. Phys. **74**, 1340 (1981); S. A. Rice and R. Kosloff, J. Phys. Chem. **86**, 2153 (1982); A. Connes, H. Narnhoffer, and W. Thirring, Commun. Math. Phys. **112**, 691 (1987).
[13] L. A. Bunimovich and Ya. G. Sinai, Commun. Math. Phys. **78**, 247, 479 (1980).
[14] L. A. Bunimovich, Commun. Math. Phys. **65**, 295 (1979).
[15] Billiard systems have completely chaotic trajectories because the curvatures of the surfaces that reflect (scatter) the point particle amplify the difference between incident and outgoing trajectory directions. Note that these systems have completely chaotic dynamics and are free of the complexity due to the presence of motion in quasiperiodic islands.
[16] J. D. Meiss and E. Ott, Phys. Rev. Lett. **55**, 2741 (1985).
[17] P. Gaspard and X.-J. Wang, Proc. Natl. Acad. Sci. USA **85**, 4591 (1988).
[18] L. S. Rodberg and R. M. Thaler, *Introduction to the Quantum Theory of Scattering* (Academic, New York, 1967).
[19] J.-P. Eckmann and D. Ruelle, Rev. Mod. Phys. **57**, 617 (1985).
[20] V. I. Oseledec, Moscow Math. Soc. **19**, 197 (1968).
[21] W. Krieger, Trans. Am. Math. Soc. **149**, 453 (1970).
[22] B. Mandelbrot, *The Fractal Geometry of Nature* (Freeman, San Francisco, 1982).
[23] L.-S. Young, Ergod. Theory Dynam. Syst. **2**, 109 (1982).
[24] H. Kantz and P. Grassberger, Physica D **17**, 75 (1985).
[25] L. P. Kadanoff and C. Tang, Proc. Natl. Acad. Sci. USA **81**, 1276 (1984); M. Widom, D. Bensimon, L. P. Kadanoff, and S. J. Shenker, J. Stat. Phys. **32**, 443 (1983).
[26] T. Bohr and D. Rand, Physica D **25**, 387 (1987).
[27] J. Machta and R. Zwanzig, Phys. Rev. Lett. **50**, 1959 (1983).
[28] L. Rosenfeld, Nucl. Phys. **70**, 1 (1965); H. M. Nussenzveig, *Causality and Dispersion Relations* (Academic, New York, 1972).
[29] R. Paley and N. Wiener, *Fourier Transforms in the Complex Domain* Am. Math. Soc. Colloquium Publ. Vol. XIX, 1934, pp. 16–17.
[30] W. Feller, *An Introduction to Probability Theory and Its Applications* (Wiley, New York, 1971).
[31] P. Szepfalusy and T. Tel, Phys. Rev. A **34**, 2520 (1986).
[32] Ya. G. Sinai, Russian Math. Surveys **27**, 21 (1972); R. Bowen, *Equilibrium States and the Ergodic Theory of Anosov Diffeomorphisms*, Lecture, Vol. 470 Notes in Mathematics (Springer, Berlin, 1975); R. Bowen and D. Ruelle, Inventiones Math. **29**, 181 (1975); D. Ruelle, *Thermodynamic Formalism* (Addison–Wesley, Reading, MA, 1978); P. Walters, *An Introduction to Ergodic Theory* (Springer, Berlin, 1981).
[33] T. C. Halsey, M. H. Jensen, L. P. Kadanoff, I. Procaccia, and B. I. Shraiman, Phys. Rev. A **33**, 1141 (1986); D. Bessis, G. Paladin, G. Turchetti, and S. Vaienti, J. Stat. Phys. **51**, 109 (1988).
[34] D. Ruelle, J. Stat. Phys. **44**, 281 (1986); W. Parry and M. Pollicott, Ann. Math. **118**, 573 (1983); M. Pollicott, Inventiones Math. **81**, 413 (1985); **85**, 147 (1986).
[35] A. Manning, Bull. London Math. Soc. **3**, 215 (1971).
[36] P. Gaspard and S. A. Rice (preprint, 1988).